The Geochronology and Stratigraphy of Comanche National Grasslands, CO

A thesis presented for distinction in geology

Alexander Olin Hager
Colorado College

May 18, 2015

TABLE OF CONTENTS

LIST OF FIGURES

ACKNOWLEDGEMENTS

First and foremost, I would like to thank my advisor Dr. Paul Myrow for getting me involved in this project, and assisting me every step of the way. His continual support and counsel has made this project what it is. I would also like to thank Dr. Bruce Schumacher, the paleontologist at the Forest Service in La Junta. Bruce accompanied me in the field, helped me collect samples, and shared his extensive knowledge of the local geology. He has been invested in determining the age and paleoclimate of these rocks for much longer than I have, and I am grateful to have worked along side of him. I am also grateful to Dr. Jahan Ramezani, a research scientist at MIT, who also accompanied me in the field, and was responsible for processing many of the samples used for radiometric dating. Additionally, I would like to thank Dr. Henry Fricke, who helped with the interpretation of my data isotope data, and Lauren Dangles, who shared some of her stable isotope data of the Morrison Formation from her senior project last year. Finally, I would like to acknowledge Dr. Sam Bowring at MIT, Dr. David Fike at Washington University, Spectrum Petrographics, and the LaserChron Laboratory at the University of Arizona for processing my samples in their laboratories.

ABSTRACT

Little was previously known for certain about the age and depositional history of the strata exposed in Picket Wire Canyon in Comanche National Grasslands, CO, as prior work in developing a comprehensive geochronology and stratigraphy of the area has been minimal. Previous age constraints for the strata have been largely speculative, as the canyon contains the only outcrop of Paleozoic–Mesozoic strata within 100 km, and correlating local strata to regional formations is troublesome. Prior chronostratigraphic constraints were based entirely on fossils in Late Triassic and younger strata, but there have not previously been age constraints for strata older than the Late Triassic Chinle Formation. Radiometric U/Pb dating of detrital and volcanic zircon grains, along with carbon and oxygen stable isotope geochemistry, were employed in this study to constrain ages of the strata in Picket Wire Canyon, as well as determine depositional conditions. A 77 m thick eolianite unit disconformably underlies the Chinle Formation and was of unknown age; however, detrital zircons extracted from the base of the unit yielded a youngest grain of 245.5 ± 5.9 Ma, indicating the eolianite is correlative to the Triassic Red Draw Member of Jelm Formation. Additionally, this data suggests the oldest strata in the canyon, those stratigraphically below the eolianite, correlate to the Permian–Triassic Lykins Formation. U/Pb dating of volcanic ash in the Ralston Creek Member of the Morrison Formation yields an age of 152.987 ± 0.063 Ma, which is the most precise age for the Morrison Formation known to date. $\delta^{13}C$ and $\delta^{18}O$ values of Morrison carbonate beds indicate deposition in an arid, hydraulically open lacustrine setting, and are consistent with previous results from other Morrison localities. The Lower Morrison Formation at this locality contains one of the world's largest continuously mapped

dinosaur trackways. These footprints are atypical in that they are preserved in oolite, which due to its granular texture should not theoretically preserve footprints. Thin section analysis of the oolite depicts microbial films both within and surrounding the ooids, along with cementation structures indicative of meteoric vadose diagensis. It is hypothesized that the presence of microbial films and diagenetic cements allowed for the preservation of the footprints by increasing cohesion between grains, thus permitting the imprints to maintain their mold indefinitely.

INTRODUCTION

Comanche National Grasslands (CNG), located in southeastern Colorado, has appeared occasionally in the geological literature since 1896 (Cragin, 1896); however, no comprehensive stratigraphy or geochronology has been developed for the area. Most of the geological research in CNG has been focused on the abundance of dinosaur tracks and fossils in the younger strata, and the older strata has largely been overlooked, despite constituting most of the exposed section. The ages of the oldest strata (latest Paleozoic–Jurassic) of CNG were previously ill defined, as they were based entirely on fossils, which have not been found in the lowest 127 m of the section (Late Triassic and older). Additionally, the study area is surrounded by grassland with no other outcrops of similar age within 100 km (Heckert et al., 2012), which makes correlation with other regional outcrops difficult. While tentative ages are known for the Jurassic Ralston Creek and Lower Morrison formations at CNG, they are largely imprecise and based on ages of other localities.

The topmost beds of the studied section include the world's largest dinosaur trackway site (Lockley et al., 1986). The dinosaur footprints are preserved in oolite, which is puzzling because ooids are granular and lack sufficient cohesion to preserve imprints. Despite the importance of this site, no research has been conducted as to why these footprints were preserved in the rock record.

As is apparent, there is still considerable uncertainty concerning the strata of CNG, and the area is in need of a comprehensive study. Such a study is important because CNG is the only outcrop of similar age in southeastern Colorado, and thus it would provide insight to the overall geologic history of Colorado and the western Great Plains region.

The objective of this study is to constrain the ages of oldest strata, correlate them to regional formations, and to develop depositional history for the section. Additionally, this study seeks to solve the odd taphonomic problem associated with the preservation of dinosaur footprints in oolite. Stable isotope geochemistry, U/Pb radiometric dating, thin section analysis, and field techniques will be employed to investigate these objectives.

STUDY AREA

Comanche National Grasslands is located in southeastern Colorado, approximately 40 miles south of the town of La Junta (Fig. 1A). Here, the Purgatoire River incised through a gently dipping local monoclinal structure, formed as a result of Laramide stresses, exposing Cretaceous and older strata in the Picket Wire Canyon (Lockley et al., 1986). The focus of the study is on the latest Paleozoic-Jurassic strata of Picket Wire Canyon. The section is divided into four localities at which it was measured (Fig. 1B). From oldest to youngest these are: the Bravo Creek Canyon section (BCC), which consists of marine and fluvial deposits of unknown age; an eolianite unit (BCC-2) also of unknown age, the Purgatoire Ralston Creek section (PRC), consisting of both the Ralston Creek and Lower Morrison formations; and the Purgatoire Footprint Sample section (PFS), which contains the world's largest continuously mapped dinosaur trackway. The PFS trackway includes over 1,300 footprints of both quadrupedal and bipedal dinosaur (Lockley et al., 1986)

Some fieldwork was also done along the Highway 24 road cut at Red Rocks Open Space (RROS section) in Colorado Springs, CO, which consists of the Lykins, Ralston Creek, and Lower Morrison formations. Samples for stable isotope analysis were collected from the Lykins and Lower Morrison formations and serve as a comparison to the Morrison strata and potential Lykins equivalents at CNG. The Lower Morrison samples from this locality were collected by Dangles (2014).

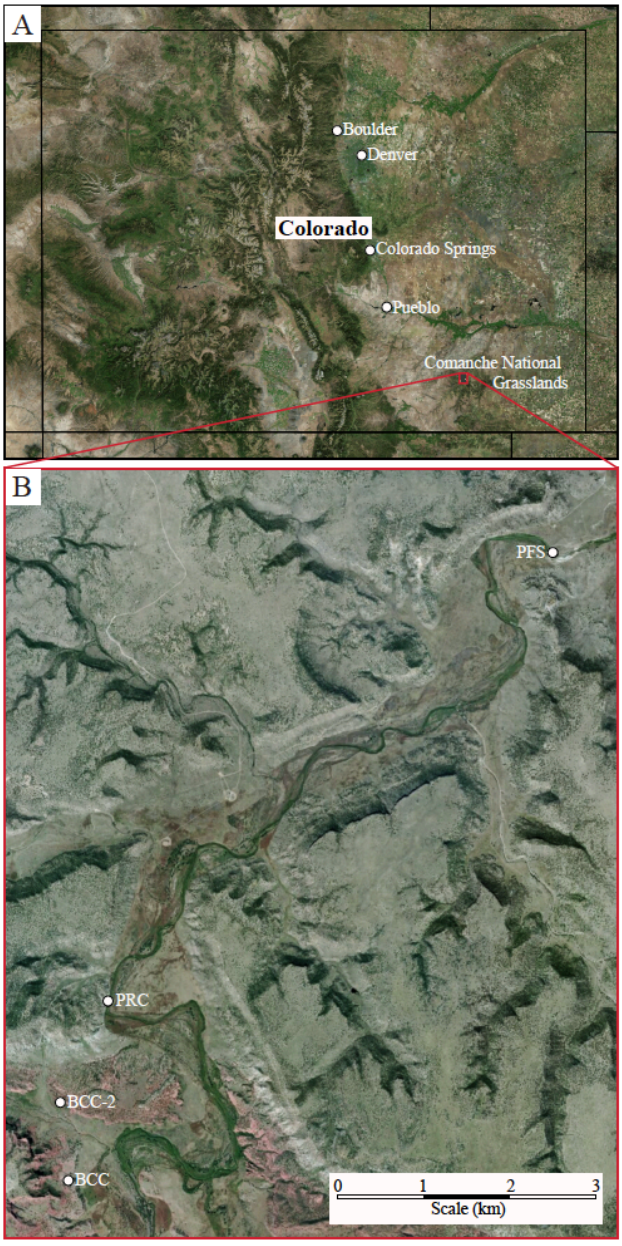

Figure 1:
A) Satellite image of Colorado showing location of Comanche National Grasslands (study area enlarged).

B) Enlarged satellite image of study area in Comanche National Grasslands including locations where each section was measured.

BACKGROUND

Previous Age Constraints of the Strata

Previous age constraints of the strata at CNG were based entirely fossils, which have not been found in the lowest 127 m of the canyon (Fig.2). The implication of this is that any preceding age estimate for these strata has been speculative. The eolianite composing the BCC-2 section was originally interpreted to be the Middle Jurassic Entrada Sandstone (Mckee et al., 1956). However, this designation was recently discredited following the discovery of Upper Triassic fossils in the overlying formation, a pebble conglomerate now correlated to the Chinle Formation (Heckert et al., 2012). The discovery of Triassic fossils stratigraphically above the eolianite meant that its age and that of the underlying strata had to be reevaluated. As the Chinle Formation rests disconformably above the eolianite, it was possible that eolianite and underlying strata could be Triassic, but could also be much older. Heckert et al. (2012) tentatively correlate the eolianite to the Red Draw Member of the Jelm Formation of central Wyoming and northeastern Colorado. Most workers would consider the Jelm Formation to be Upper Triassic; however, the Red Draw Member is presently defined by the fossil of a capoitosaurid amphibian, which lived in western North America during the Middle Triassic or earlier (Heckert et al., 2012). As no maximum age constraints exist for the eolianite at Comanche National Grasslands, it is possibly much older than Lower–Middle Triassic, and could correlate to the Pennsylvanian–Permian Lyons Formation along the Front Range of Colorado.

Current ages for the strata underlying the eolianite are also ill defined, and previous ages estimates are from Middle Permian to Middle Triassic, although they may be older. It has been suggested that the stromatolitic dolomite beds found at the base of

Figure 2: General Stratigraphic Column

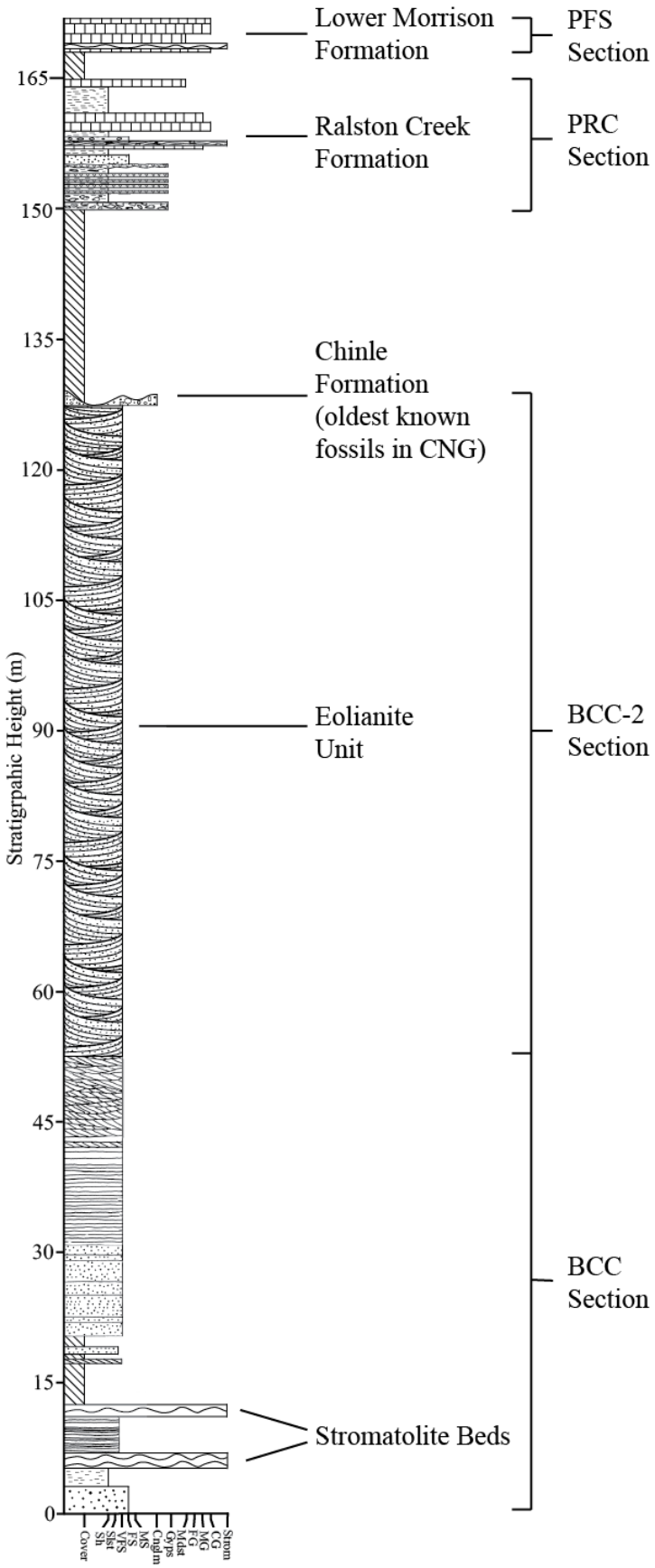

stratigraphic section correspond to either the Permian–Triassic Forrelle Limestone Member of the Lykins Formation (Heckert et al., 2012) or the Middle Permian (Guadalupian Epoch) Day Creek Dolomite (Cragin, 1896; Maughan, 1980). These correlations are only speculative, and a systematic attempt to date the lower strata has not previously been undertaken. Stromatolites are considered to be "disaster taxa," and are only abundant following mass extinctions since the rise of metazoan predation in the Phanerozoic (Schubert and Bottjer, 1992). If the stromatolite beds did coincide with the Lykins formation, they would likely represent the Permian–Triassic extinction, the largest in Earth's history.

The Ralston Creek and Lower Morrison formations are Middle–Upper Jurassic, although their exact ages at CNG are uncertain (Kowallis, 1998; Peterson and Turner, 1998; and others). The J–5 unconformity, which at CNG is located at the contact of the Ralston Creek Formation and the underlying Chinle Formation, likely represents a hiatus of 30–35 m.y.. The Lower Morrison lies stratigraphically above the Ralston Creek, and the contact between the formations is locally considered to be at a widespread blue chert bed (157.75 m–158.08 m in the overall section), which could potential represent an disconformity. At other localities, the contact between the Ralston Creek and Morrison formations is typically considered conformable, and in many places the characteristic lithologies of the two are interfingered (Peterson and Turner, 1998). In 2010, Schumacher (unpublished study) dated detrital euhydral zircons within the mudstone bed directly above the blue chert bed. U/Pb radiometric dating produced an uppermost Jurassic a mean date of 151.46 ± 3.1 Ma. Although this date has a fairly large error, it was the best constraint on the age of these strata that existed prior to this study.

Chemostratigraphy

Principles of Isotopic Fractionation:

Temporal fluctuations in stable isotope ratios of carbonate deposits can be used to correlate strata worldwide, a field called chemostratigraphy. Chemostratigraphy is based principally on global fluctuations of $^{13}C/^{12}C$ and $^{18}O/^{16}O$ that are recorded in carbonate. Isotopic fractionation occurs when a particular isotope is favorable in undergoing a chemical reaction, which is dictated by the relative size of each isotope, and which indirectly controls the bond strength of the atom or the molecule it resides in. This is illustrated using the equation for kinetic energy of a particle ($\varepsilon_k = mv^2$), where ε_k is the atomic kinetic energy, m is the isotopic mass, and v^2 is the atom's vibrational velocity, which coincides with its vibrational energy. The kinetic energy of an atom remains constant, so because m is bigger for larger isotopes, they must accommodate with a slower vibrational velocity. An atom or molecule with a lower vibrational energy requires more added energy to break its bonds, and thus forms stronger bonds than its smaller isotopic counterpart. Larger isotopes are therefore preferentially used in chemical reactions because they form stronger bonds. The degree to which this fractionation occurs at on a global scale is controlled by climate, temperature, tectonism, and biological activity. Global isotopic oscillations are recorded wherever carbonate is precipitated in equilibrium, both in terrestrial and marine environments.

Stable isotope ratios are usually written according to their δ-value, which is a ratio of the relative abundance of heavy isotope and light isotopes of the sample, compared to

that of a global standard. For example, the expression, $\delta^{18}O$, refers to the ratio of $^{18}O/^{16}O$ in the sample to that of a standard, as determined using the equation:

$$\left(\frac{\left(\frac{^{18}O}{^{16}O}\right)_{SAMPLE}}{\left(\frac{^{18}O}{^{16}O}\right)_{STANDARD}} - 1 \right) X\ 1000 = \delta^{18}O$$

Global temperature, evaporation, precipitation, and polar ice volumes are the strongest controls on global oscillations of $\delta^{18}O$ (Faure, 1998). Kinetic isotopic fractionation occurs when the system is not in equilibrium, as is the case during evaporation of water. As $H_2{}^{16}O$ molecules are smaller and have a higher vibrational energy than $H_2{}^{18}O$, they require less energy to excite them into a phase change into a gaseous state (Faure, 1998). This means $H_2{}^{16}O$ has a vapor pressure than $H_2{}^{18}O$, and is thus preferentially evaporated. The effect of this is ^{16}O-rich atmospheric water and ^{18}O-rich seawater (Keith et al., 1964). Further fractionation of water occurs during condensation, when again $H_2{}^{18}O$ is preferentially condensed to rainwater, as it requires more energy to be maintained in a gaseous state. This creates atmospheric water with even more negative $\delta^{18}O$ values. Isotopic distillation creates even more ^{16}O-rich vapor as atmospheric circulation carries water vapor toward the poles and across continents, and ^{18}O is continually preferentially condensed and rained out. The result of this is that terrestrial and polar water is far more $\delta^{18}O$ negative and variable than equatorial waters, which stay relatively constant. On average, precipitation $\delta^{18}O$ values in temperate terrestrial regions are approximately 7‰ lower than marine values at similar temperature and latitude (Clayton and Degens, 1958), but this discrepancy can reach 30‰ at high latitudes and altitudes. During cold periods when ice caps form at the poles, $H_2{}^{16}O$-rich rainwater is sequestered as ice (Maslin and Swan, 2006), raising the global $\delta^{18}O$

signature. Warm global temperatures reverse this process by melting ice caps and glaciers, and releasing the sequestered H_2O^{16} back into the ocean.

The degree of isotopic fractionation that occurs throughout these processes is influenced by temperature. This is especially true for oxygen isotope fractionation, and as such, fluctuations in $\delta^{18}O$ are typically associated in changes in temperature, and $\delta^{18}O$ values are commonly used as a paleothermometer (Maslin and Swan, 2006; Joachimski et al., 2010). At high temperatures, both $H_2{}^{18}O$ and $H_2{}^{16}O$ have high vibrational energies, and the discrepancy between the two in chemical reactions is less substantial. Conversely, at cold temperatures the difference in vibrational energies between $H_2{}^{18}O$ and $H_2{}^{16}O$ is more considerable, so more fractionation will occur that favors $H_2{}^{18}O$ in reactions.

Ocean water salinity and density, as controlled by evaporation rate and the freezing or melting ice, also have minor affects on $\delta^{18}O$ levels (Maslin and Swan, 2006), which are more substantial in terrestrial settings. An increase in either salinity or density causes an eventual increase in $\delta^{18}O$. Due to the massive volume of the ocean, marine $\delta^{18}O$ fluctuations are usually minor and do not vary more than 2.0‰ (Clayton and Degens, 1958).

Carbon isotope fractionation is more complex than oxygen, and is primarily a function of biological processes (Clayton and Degens, 1958; Maslin and Swan, 2006), and to a lesser extent ocean circulation, atmospheric and oceanic temperature, ocean pH, and global chemical weathering rates. During photosynthesis, marine plants preferentially use $^{12}CO_2$ over $^{13}CO_2$ by up to 25‰ (Maslin and Swan, 2006), because it requires more energy to break apart the stronger $^{13}CO_2$ bond. This results in ^{13}C-poor organisms and ^{13}C-rich seawater. $\delta^{13}C$ values in marine plants typically fall in the range of –8‰ to –

17‰ (Craig, 1953). Oxidation of organic matter releases ^{12}C back into the inorganic carbon reservoir (Clayton and Degens, 1958), and thus negative excursions of $\delta^{13}C$ can coincide with mass extinctions and an increase in organic decay. Carbonate forming in equilibrium with ocean water typically has $\delta^{13}C$ values of 2‰ to 2.5‰ (Mook, 2001), but could vary from –4‰ to 4‰ (Clayton and Degens, 1958) in normal marine conditions.

$\delta^{13}C$ values in freshwater carbonate deposits are generally more varied and more negative than their marine equivalents. In a study by Keith and Weber (1964) of 321 marine carbonate and 183 freshwater carbonate samples, 85% of marine carbonate samples had $\delta^{13}C$ values greater than –2‰, while 84% of freshwater samples had $\delta^{13}C$ values less than –2‰. $\delta^{13}C$ values of marine plants typically vary from –8‰ to –17‰, whereas terrestrial plants usually range from –22‰ to –29‰ (Craig, 1953). This discrepancy is because terrestrial plants acquire CO_2 through stomata, while marine plants absorbed CO_2 through diffusion across the cell wall. Obtaining CO_2 through stomata is a more efficient process, and allows terrestrial plants to be more selective in using $^{12}CO_2$ for photosynthesis. Terrestrial plant respiration and oxidation of humus releases CO_2 and bicarbonate with an average $\delta^{13}C$ value of –25‰ into the soil, and thus groundwater, streams, and lakes also have much lower $\delta^{13}C$ than seawater (Keith and Weber, 1964). Terrestrial $\delta^{13}C$ values are also affected by atmospheric CO_2, rainwater composition, and fluvial input $\delta^{13}C$ values, which reflect the composition of the eroded rock. These factors contribute to the greater variability in $\delta^{13}C_F$ values observed in lacustrine than marine carbonate.

Temperature and acidity affect the overall amount of carbon that enters or exits the ocean as CO_2 or carbonate, while carbon burial during chemical weathering and ocean

plate subduction affects the total amount of carbon in the system. While these processes are not primary controls on the degree of carbon isotope fractionation that occurs, they can indirectly affect $\delta^{13}C$ values by influencing biological activity or burial of particularly ^{12}C-rich or ^{12}C-poor rock or sediment.

The hydrology of lakes has a major influence on the $\delta^{18}O$ and $\delta^{13}C$ composition of lacustrine carbonate. Lake water in hydraulically open basins has a relatively short residence time for lake water, and as a result, $\delta^{18}O$ and $\delta^{13}C$ values reflect those of fluvial input, as determined by rainwater composition and organic oxidation. Open basins show little or no variation in $\delta^{18}O$ values (Talbot, 1990), as $\delta^{18}O$ values for rainwater remain fairly constant at a given locality. $\delta^{18}O$ and $\delta^{13}C$ values in open systems are controlled by the different factors, and therefore show very little correlation (correlation coefficient, $r < 0.7$; Talbot, 1990; Dunagan and Turner, 2004). The isotopic composition of hydraulically closed basin lake water is distinctly different from open basins in that $\delta^{18}O$ and $\delta^{13}C$ values are closely correlated ($r \geq 0.7$; Talbot, 1990; Dunagan and Turner, 2004). Closed lake systems have long residence times for lake water, and evaporation is the principal way water and carbon can exit the system. Preferential evaporation of the lighter $H_2{}^{16}O$ and $^{12}CO_2$ molecules creates isotopically heavy lake water, which is then reflected in carbonate (Talbot, 1990). In closed systems organic oxidation, isotopic content of precipitation, and temperature are of secondary importance to preferential evaporation (Talbot, 1990), which is responsible for the close correlation.

Although lacustrine carbonate deposits are more variable and more negative in isotopic composition than marine carbonate, they can reflect global $\delta^{13}C$ signatures, as observed in lacustrine carbonate deposits from the Triassic Germanic Basin (Korte et al.,

2010). Two negative $\delta^{13}C$ excursions exist in these deposits near the P–T boundary, which correspond to the global marine record. A shift in the carbon cycle originating in any of the biosphere, atmosphere, lithosphere, or hydrosphere reservoirs will be reflected in the other reservoirs almost instantaneously through mass transport by rivers, evaporation, precipitation, and atmospheric and ocean circulation.

Permian–Triassic Chemostratigraphy:

Corsetti et al. (2005), Galfetti et al. (2007), Joachimski et al. (2012), Saltzman and Sedlacek (2013), Korte et al. (2010), and others provide $\delta^{13}C$ data for Upper Permian to Middle Triassic strata from localities worldwide (Fig. 3). Global patterns indicate a sharp negative $\delta^{13}C$ excursion just before the P–T boundary, succeeded by 4–6 m.y. of fluctuation, eventually stabilizing in the Middle Triassic. Tectonic influences were not responsible for the degree of $\delta^{13}C$ fluctuation, as no outstanding continental rearrangement occurred along the P–T transition except for the northwesterly translation of Pangea (Galfetti et al., 2007). The fluctuation of this time period is considered a result of the large-scale volcanism of the Siberian Traps and associated increase in atmospheric CO_2 levels, and a subsequent rise in surface water temperatures of 8°C (Joachimski et al., 2012).

An initial negative $\delta^{13}C$ excursion associated with the P–T boundary lasted approximately 500,000 years in the Changhsingian Stage of the uppermost Permian (Korte et al., 2010; Corsetti et al., 2005). The extent of the excursion varies, but global $\delta^{13}C$ values are described as decreasing from ~2–4‰ to ~–1‰ (Corsetti et al., 2005), or having an average decline of 4–7‰ (Korte et al., 2010). The rising limb of the brief $\delta^{13}C$

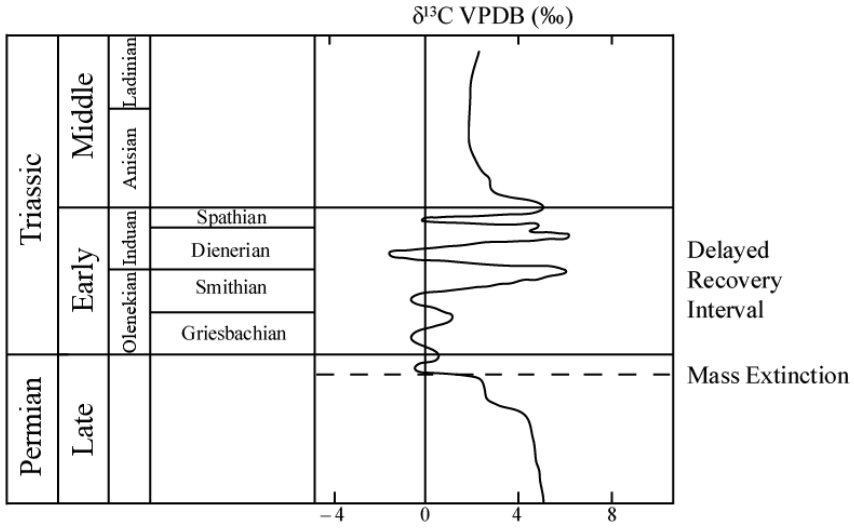

Figure 3: Modified figure from Corsetti et al. (2005). Graphs depicts global carbon and strontium isotope fluctuations from the Late Permian to the Middle Triassic. Massive and rapid carbon isotope flucatuations occur throughout the latest Permian and Early Triassic, before eventually stabalizing in the Middle Triassic.

excursion in the uppermost Permian is present just below the marine extinction horizon, indicating that this initial negative excursion was not a result of the P–T extinction itself, but was perhaps caused by another factor such as volcanism (Korte et al., 2010). $\delta^{13}C$ values show a mild decrease again in the Upper Griesbachian Substage (Induan Stage) of the lowermost Triassic, but return to positive values by the Greisbachian–Dienerian substage boundary in the middle Induan Stage (Corsetti et al., 2005). The Middle Dienerian marks another decrease in $\delta^{13}C$ values, which is followed by yet another positive trend for the remainder of the Dienerian (Corsetti et al., 2005).

The Induan–Olenekian stage boundary in the Early Triassic marks the beginning of extremely rapid and vast fluctuations. The Smithian substage of the Olenekian (Early Triassic) marks a return to negative $\delta^{13}C$ values. Smithian $\delta^{13}C$ values are as low as –4‰ in the Thaynes Formation, NV (Saltzman and Sedlacek, 2013), and are followed by a drastic positive excursion along the Smithian–Spathian Substage (middle Olenekian Stage) boundary. Values in this interval reach $\delta^{13}C_M$ of ~3‰ in south China and northern India (Galfetti et al., 2007), and are as heavy as ~7.5‰ in the Confusion Range, Utah (Saltzman and Sedlacek, 2013). This positive excursion is associated with an increase in burial of ^{12}C-rich organic matter (Galfetti et al., 2007). A similar spike in $\delta^{13}C$ values occurs on the Spathian–Anisian (Early–Middle Triassic) boundary after a brief interval of negative $\delta^{13}C$ values in the Spathian (Corsetti et al., 2005; Galfetti et al., 2007). $\delta^{13}C$ values eventually stabilize in the Anisian stage of the Middle Triassic after the 4–6 m.y. period of $\delta^{13}C$ oscillations (Corsetti et al., 2005). Of all the $\delta^{13}C$ late Permian–Early Triassic $\delta^{13}C$ excursions, the Spathian–Anisan and the Smithian–Spathian excursions are

considered the best stratigraphic markers, as they are the most drastic and pervasive globally (Galfetti et al., 2007).

Chemostratigraphy of the Morrison Formation:

Published data for the lacustrine and palustrine deposits of the Morrison Formation have values of $\delta^{13}C$ of –2.6‰ to –8.8‰, and $\delta^{18}O$ values of –8.3‰ to –12.9‰ (Dunagan and Turner, 2004). The correlation coefficients for $\delta^{18}O$ to $\delta^{13}C$ comparisons for the Morrison Formation are variable (r=0.5–1.0), and have been classically been interpreted as open-system lacustrine deposits (Talbot, 1990; Dunagan and Turner, 2004). Dunagan and Turner (2004) point out that open-systems are typically associated with considerable fluvial inputs, which is inconsistent with sedimentological, paleontological, and paleoclimatic data for the Morrison that support an arid climate. They therefore suggest deposition occurred in a hydraulically open basin that was largely groundwater fed, resulting in a lake/wetlands environment with more significant variability in $\delta^{18}O$ values. They divide the lacustrine Morrison deposits into three categories based on sedimentological characteristics and somewhat overlapping isotopic ratios: 1) lacustrine/palustrine deposits near the shoreline with $\delta^{18}O$ and $\delta^{13}C$ values of –8.3‰ to –11.8‰ and –2.7‰ to –7.03‰, respectively; 2) lacustrine/palustrine deposits distal to the shoreline with $\delta^{18}O$ and $\delta^{13}C$ values of –8.3‰ to –9.9‰ and –2.6‰ to 4.3‰, respectively; and 3) undifferentiated deposits with $\delta^{18}O$ and $\delta^{13}C$ values of –8.2‰ to –12.9‰ and –2.5‰ to –8.8‰, respectively. Dunagan and Turner (2004) describe marginal deposits of the Morrison as composed of oolitic and skeletal packstone to grainstone, siltstone, and sandstone, and distal deposits as skeletal mudstone to wackestone,

microbialites, and laminated siliciclastic mudstone. They consider deposits of chert and evaporites as having formed in temporarily saline or alkaline shallow water settings.

Paleozoic–Triassic Detrital Zircon Spectra

U/Pb ages of detrital zircons (DZ) in sedimentary rock are a useful tool for constraining the maximum age of strata, as well as determining the ultimate source rock of the grains. DZ grains are mainly incorporated into sedimentary strata by erosion of igneous basement rock, but can also happen by ash fall. DZ data are presented as age probability plots, which show the relative abundance of zircon ages of grains in a sample. Peaks in the probability plot corresponds to a particular source rocks, and the youngest zircon age provides a maximum age constraint for the stratum. Strata of similar age in a particular region are usually derived from the same source rock, and therefore have comparable probability plots. DZ spectra of Paleozoic to Triassic strata in the western North America indicate six different igneous sources of the following ages: (1) Archean (~ 3300–2550 Ma), (2) Paleoproterozoic (~ 2000–1600 Ma), (3) Mesoproterozoic (~ 1250–950 Ma), (4) Cryogenian to Ediacaran (~ 665–565), and (5) Paleozoic (~ 495–310 Ma; Link et al., 2014; Dickinson and Gehrels, 2003; Dickinson and Gehrels, 2010; Gehrels and Pecha, 2014). Generally, approximately 75% of DZ grains in Paleozoic strata are derived from Archaen, Proterozoic, and Paleozoic basement rocks along the Appalachian Mountains that were transported west by large-scale fluvial systems (Dickinson and Gehrels, 2003; Link et al., 2014). The other 25% of DZ grains originated from local Mesoproterozoic basement rock that eroded off of the Ancestral Rocky Mountains (ARM) in the Paleozoic. The concentration of ARM DZ grains is greatest in

Permian and Pennsylvanian strata and gradually diminishes over time (Dickinson and Gehrels, 2003). This is because the ARM were at their highest elevations in the Pennsylvanian and Permian, and were only minimally exposed in the Triassic and Jurassic.

METHODS

Measurement of Strata

Sections were measured at four localities within a 4 km radius in June of 2013. Measurements were made using a staff and tape measure, and lithology, grain size, sedimentary structures, texture, thickness, and color of each unit were noted. The BCC section is 50.21 m thick, the eolianite unit at BCC-2 is 77 m thick, the PFS section is 18.39 m thick, and the PRC section is 3.42 m thick. Including all covered intervals, the total thickness of strata measured in this study is 172.53 m.

Radiometric U/Pb Dating

High precision radiometric U/Pb dating of zircons was used to determine age constraints for strata in the BCC, BCC-2, and PRC sections. Zirconium silicate ($ZrSiO_4$), or zircon, is a mineral formed in silicic igneous melts. Similar atomic diameters of zirconium and uranium allows for the occasional substitution of uranium for zirconium during crystallization. Uranium radioactively decays at a constant rate into lead, which due to its larger atomic diameter, does not otherwise fit into the zircon crystal lattice, and cannot act as a substitute for zirconium during crystallization. It can therefore be safely assumed that any lead isotopes in zircon are radiogenic, thus making it possible to determine the age of zircons based on the ratio of uranium to lead in zircons and the half-life of decay.

There are two lead isotopes that form from radiogenic decay of uranium: ^{206}Pb, which decays from ^{238}U with a half-life of 4.47 b.y., and ^{207}Pb, which decays from ^{235}U with a

half-life of 0.704 b.y. (Dickins, 1995). Ratios of both isotopes can be used to calculate the age of zircon using the following equations (Dickins, 1995):

$$^{206}Pb_P = {}^{206}Pb_I + {}^{238}U\ (e^{\lambda_{238}t} - 1)$$

$$^{207}Pb_P = {}^{207}Pb_I + {}^{235}U\ (e^{\lambda_{235}t} - 1)$$

where Pb_P is the abundance of ^{206}Pb or ^{207}Pb in the zircon, Pb_I indicates the initial abundance of ^{206}Pb or ^{207}Pb, λ is the decay constant (1.55125×10^{-10} for $^{238}U \rightarrow {}^{206}Pb$ and 9.8485×10^{-10} for $^{235}U \rightarrow {}^{207}Pb$), and t is time in years. Zircons have negligible $^{206}Pb_I$ and $^{207}Pb_I$ values, so the equations are typically simplified to:

$$^{206}Pb = {}^{238}U\ (e^{\lambda_{238}t} - 1)$$

$$^{207}Pb = {}^{235}U\ (e^{\lambda_{235}t} - 1)$$

Radiometric zircon analysis was undertaken for both volcanic ash deposits and detrital grains in sedimentary rocks. Volcanic ash beds in the sedimentary record are extremely useful for geochronological analysis, as they provide well-preserved, primary zircons that accurately represent the age of the strata in which they reside. It is possible to incorporate zircons from ash fall into low-energy depositional facies. This means lacustrine mudstone, siltstone, limestone, and sandstone have the potential to provide accurate radiometric ages in strata where a complete ash bed does not exist. Detrital zircons are derived principally from igneous and volcanic source rocks, and they contain a wide range of U/Pb ages, which are shown on a relative age probability plot. Detrital zircons only provide a maximum age constraint for the sampled strata, not the depositional age.

Six samples were collected throughout the strata for dating. Lithologies of samples include sandstone, silty mudstone, and volcanic ash. Three samples of silty mudstone

were collecting along an oxidized layer at 20.35 m in the BCC section. One sample of volcanic ash was processed for U/Pb radiometric dating from a bed just below the blue chert layer that marks the top of the Ralston Creek Formation (155.4 m). One sandstone sample was collected for detrital zircon analysis from the eolianite unit at BCC-2, approximately 3 m from its base. Samples were carefully extracted to avoid contamination by detritus in adjacent beds, and were approximately 10 cm^3 in size.

Samples from BCC and PRC were sent to the radiogenic dating lab at Massachusetts Institute of Technology (MIT). Samples are broken down into monomineralic fragments as small as 10 μm by pulverization and sonication. The magnetic minerals were removed using Franz magnetic separator. Zircon and other dense minerals are isolated in the dense liquids Bromoform or Methylene Iodide. Individual zircon grained with the most intact euhydral structures were handpicked for mass spectrometry using a VG Sector 54 mass spectrometer. Results are corrected for fractionation, blank, spike, and initial U/Th disequilibrium.

A detrital zircon sample from BCC-2 was sent to the Arizona LaserChron Center at the University of Arizona at the University of Arizona geochronological analysis. 248 zircon grains were randomly selected without bias to shape, size, or color. The DZ grains were mounted on epoxy plugs and polish to half thickness, and were laser ablated using an ArF Excimer DUV193 using a wavelength of 193 nm. The ablated material was then transported in helium gas into the multicollector inductively coupled plasma mass spectrometer to determine relative isotope ratios.

Thin Section Analysis

Microscope analysis of six thin sections of the PFS oolite beds was used to investigate the depositional history of the oolite, and to solve the taphonomic enigma of dinosaur footprint preservation in oolite. Spectrum Petrographics Inc. in Vancouver, WA mounted standard, polished thin sections for use in this study.

Carbonate $\delta^{13}C$ and $\delta^{18}O$ Analysis

Samples for $\delta^{13}C$ and $\delta^{18}O$ analysis were collected from carbonate at the base of the BCC section, and throughout the PRS and PFS sections. Samples were collected from fresh, clean surfaces, and were approximately 3–5 cm^3 in size. Thirty samples were collected from the BCC section, 16 samples from the PFS section, and 11 samples from the PRC section. Carbonate samples collected by Dangles et al. (2014) from Morrison Formation in Red Rock Open Space, Colorado Springs, CO were also analyzed. Additionally, 8 carbonate samples from the Forrelle Member of the Lykins Formation at Red Rock Open Space were used as a comparison to the BCC carbonate. Fresh surfaces were cut into the samples, which were then drilled to extract approximately 100μg of powder. The powdered samples were then sent to Dr. David Fike's Stable Isotope Geochemistry Laboratory at Washington University in St. Louis. At the laboratory, the samples were sealed with helium in air-free tubes, and reacted with H_3PO_4 for 4 hours at 72 °C. The expelled CO_2 was sampled with a Finnigan Gas Bench II. The stable isotope ratios were then determined using either a Finnigan MAT 252 or Delta V Plus mass spectrometer. The mass spectrometer removes the outermost electrons from the molecules, yielding positively charge ions. The ions are then separated in a magnetic

field according to mass. Final $\delta^{13}C$ and $\delta^{18}O$ ratios are expressed in per mil units, and are standardized to the Vienna Pee Dee Beleminite (VPDB).

FACIES DESCRIPTIONS

The oldest strata in the area are exposed at the Bravo Creek Canyon (BCC) section (Fig. 4), and have previously been interpreted as the Forrelle Limestone Member of the Lykins Formation (Heckert et al., 2012), or the Day Creek Dolomite (Cragin, 1896; Maughan, 1980). The lowermost 3.01 m consists of red very fine-grained sandstone, with cryptic bedding that is 0.5–1.0 cm thick. The upper 40 cm of this unit is speckled with white and gray reduction spots. From 3.01 m to 5.15 m there is orange claystone with minor siltstone beds. Above this is a 47 cm thick covered interval. At 5.62 m, there is the first of two stromatolitic dolostone beds in this unit (Fig. 5). This stromatolitic unit is 1.45 m thick, with 3–16 cm thick beds and 1–4 cm thick lenticular calcisiltite to mudstone beds between mounds. The stromatolite unit is succeeded by 2.52 m of red–orange, very thinly bedded (average = 5 mm) claystone and red–maroon siltstone. At 9.70 m is a 76 cm interval of purple, very fine-grained sandstone. The lower 43 cm of this unit has predominately thin (~5 cm), tabular beds, with scattered wavy ripple cross-lamination. In the upper 33 cm, the unit transitions into trough cross-bedded (beds = 2–5cm) very fine-grained sandstone rich in carbonate. Above this unit (at 10.51 m) is 56 cm of ripple cross-laminated, fine and medium dolograinstone beds up to 9 cm thick (average = 5 cm), with a few thin lenses of carbonate dolomudstone. This unit transitions into the second stromatolitic dolostone unit at 11.07 m. The stromatolite is brown to white, and has beds 4–15 cm thick, with laminated intervals 2–4 mm thick. The lower 54 cm has predominately parallel microbial lamination to very low relief mounds, with more distinctive stromatolitic texture at the top of the unit. Above the stromatolite unit is 7.77 m of cover, with minor outcropping of red–orange, very fine-grained sandstone, siltstone,

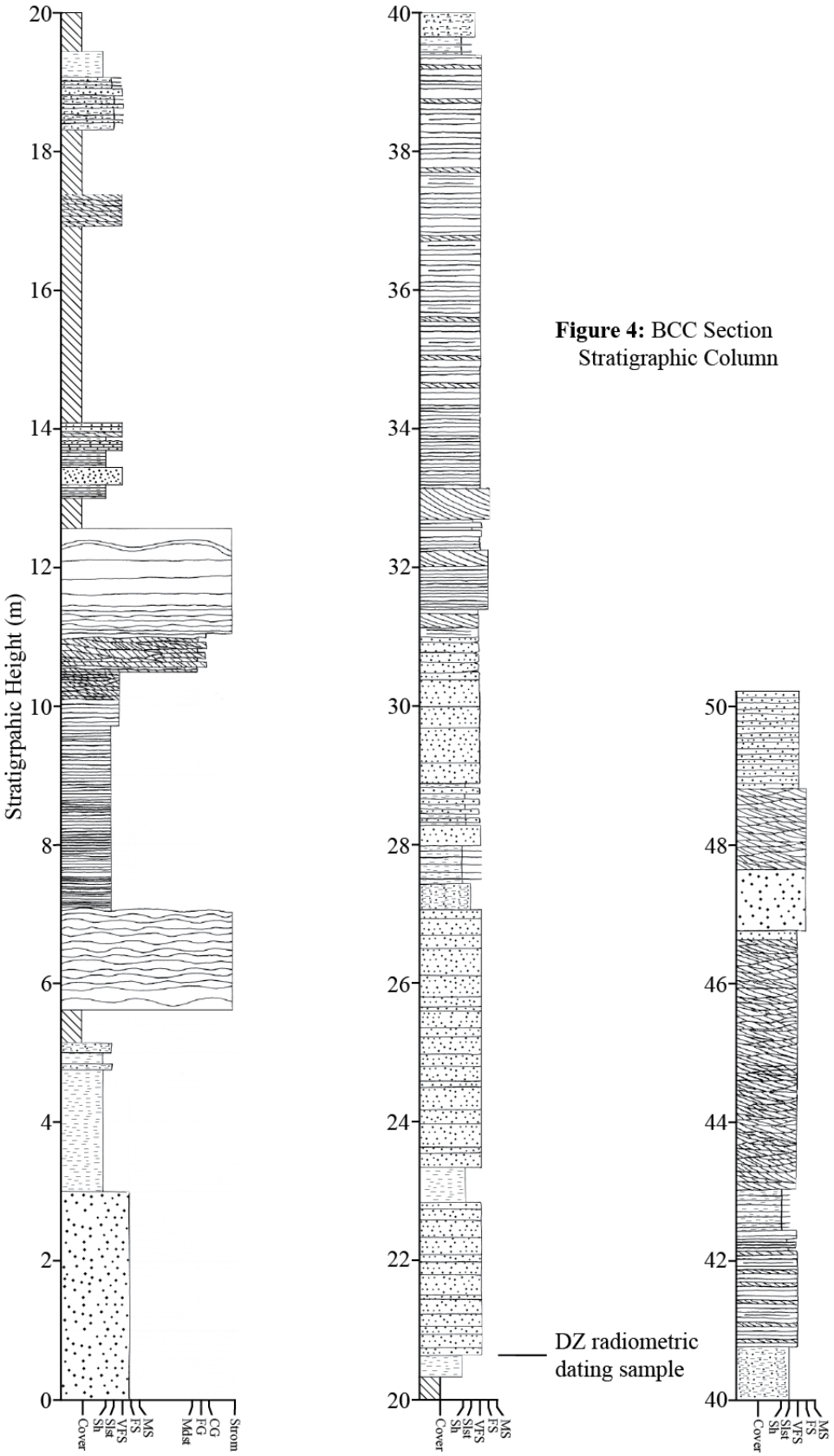

Figure 4: BCC Section Stratigraphic Column

Figure 5: Stromatolite beds in BCC unit. A) The lower stromatolite bed showing some displacement of the laminae along minor fault. Pencil is 15 cm long. B) Both stromatolite beds and associated red fine sandstone beds in the lower Bravo Creek Canyon section. The rock hammer rests on the lower stromatolite bed (at 5.62 m). The uppermost bed pictured is the second stromatolite bed (at 11.07 m). Hammer is 33 cm long. C) Very thin, tabular mudstone, claystone, and siltstone beds (~9.50 m). Tip of pencil is 2 cm long.

or shale. One of the sandstone intervals (at 13.70 m) has wave ripple lamination, and mudcracks outcrop in two sandstone beds (at 13.75 m and 13.96 m). One 45 cm thick sandstone unit (16.83 m) has ripple cross-laminated beds in sets 1–3 cm. Above the covered interval (at 20.35 m) is a 30 cm thick red shale unit with a discontinuous, < 6 cm thick white reduction band.

The section from 20.35 m to 50.21 m is dominated by alternating thin to massively bedded, very fine-to-fine-grained sandstone, with some shale and siltstone beds (Fig. 6). The unit is dark red, maroon, and orange in color, and contains 10 cm to 5.05 m thick beds and bed sets, with an average of 1 m. Mudcracks exist at 27.83 m and 43.15 m, with the first containing multigenerational mudcracks throughout 17 cm of strata. There is trough cross-bedding at 31.0 m, 43.02 m, and 47.67 m in units 41 cm, 3.6 m, and 1.38 thick, respectively. The lower unit has cross-bed set thicknesses up to 26 cm, while the upper two units each have sets 3–20 cm thick average 6–8 cm thick). Two isolated beds of orange, fine-grained sandstone with large, dune-sized cross-bedding occur at 32.03 m and 32.69 m, with thicknesses of 23 cm and 47 cm. Ripple cross-lamination is preserved in units at 34.35 m and 40.48 m, with thicknesses of 5.05 m and 1.37 m, respectively. The unit at 34.35 m has ripple sets 2–10 cm thick, and the unit at 40.78 m has 1–5 cm thick sets.

The BCC-2 eolianite unit (77 m thick) at 50.21 m was briefly measured at a section ~900 m northwest of the BCC section (Fig. 2). The eolianite is mostly orange, but has a distinctive maroon basal unit of large spherical nodules formed from weathering (Fig. 7). Wind ripple lamination is abundant in the large dune-scale cross-lamination of the

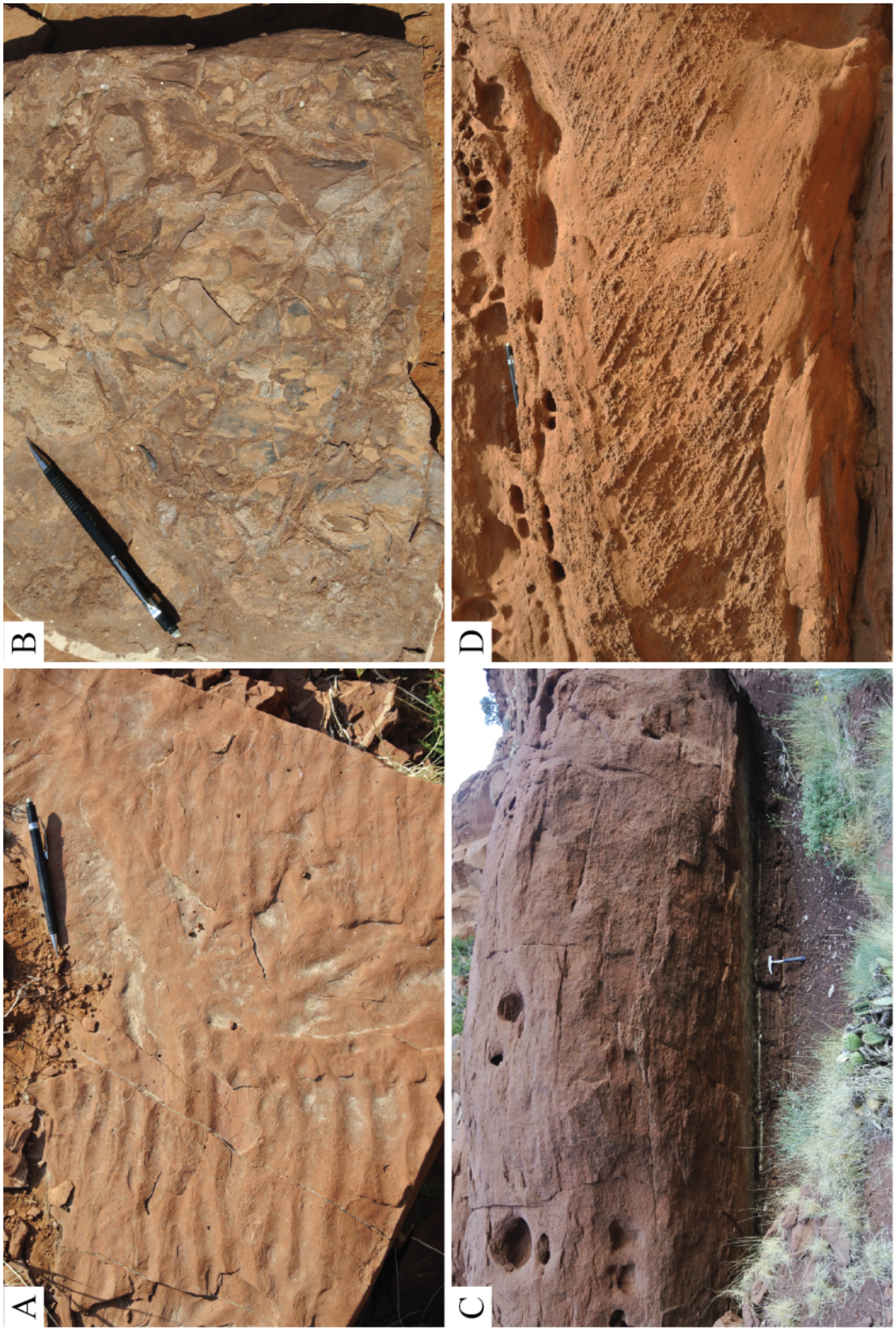

Figure 6: A) Symmetrical ripples with bifurcations exposed on bedding plane (16.83 m). B) Large polygonal mudcracks (27.83 m). C) White reduction band or volcanic ash bed in mudstone/siltstone bed (20.35 m) that was sampled for radiometric dating. Hammer is 33 cm long. D) Orange, fine-grained sandstone with dune-scale cross-bedding (32.67 m). Pencil in A, B, and D is 15 cm long.

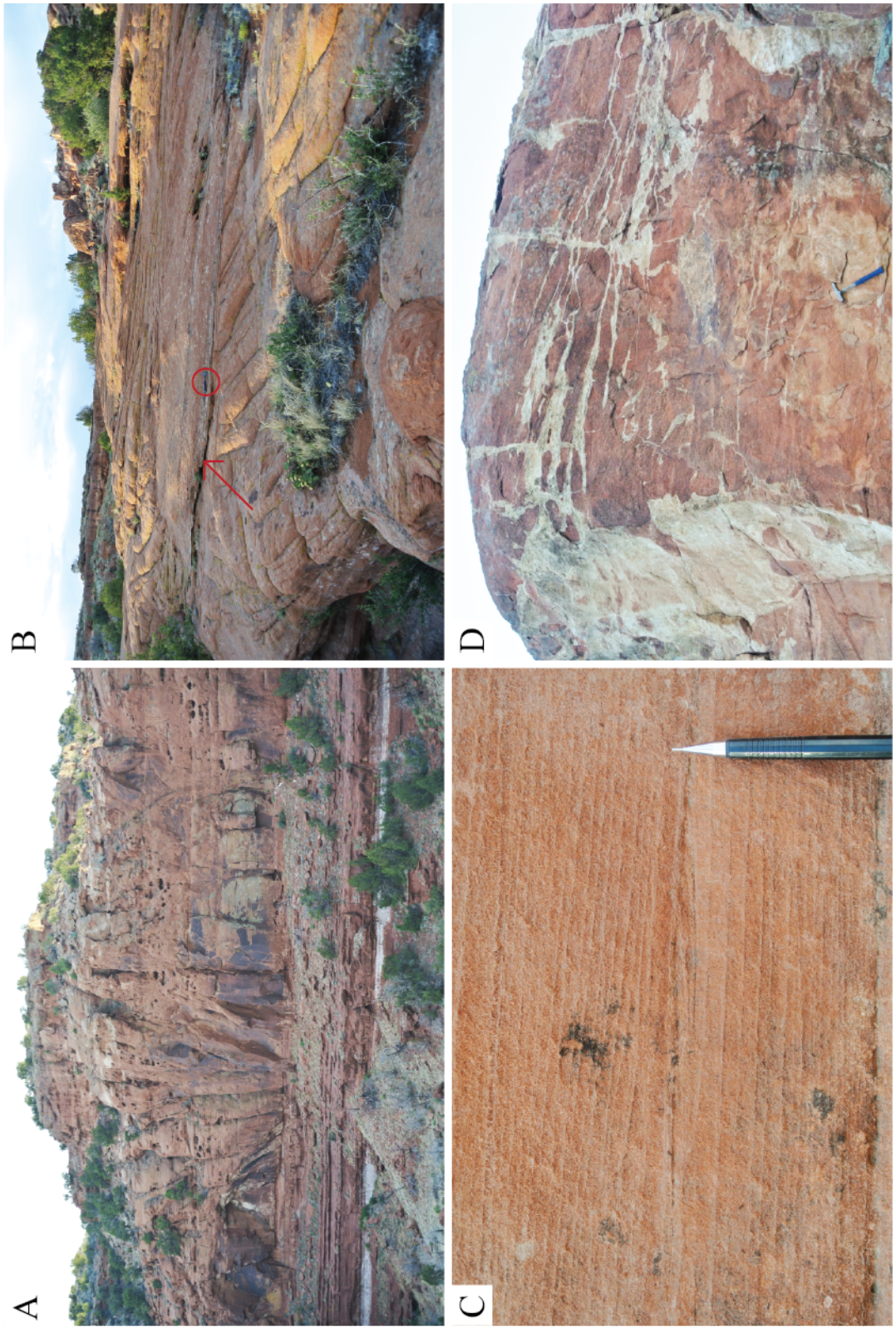

Figure 7: A) A view of pink-tan eolianite unit (77 m thick) resting on thinner-bedded red strata. B) Possible supersurface (arrow) within dune-scale cross-bedding. Hammer for scale (circled) is 33 cm long. C) Subcritical, climbing translatent strata, produced by wind ripples. Tip of pencil is 2 cm long. D) White, polygonal weathering fractures in top 5 m of eolianite. Hammer is 33 cm long.

eolianite. The top 5 m of the eolianite contains large polygonal cracks that are white from iron reduction.

Disconformably above the eolianite, at 127 m, is a limestone pebble conglomerate unit, which has been tentatively correlated to the Chinle Formation (Heckert et al., 2012), and which varies in thickness from 0 m to ~2 m (Fig. 8). Bone and tooth fragments indicative of Upper Triassic tetrapod taxa, as well as a *ganoid osteichthyan* scale, exist in this unit (Heckert et al., 2012) and are rounded, abraded, and fractured.

The Ralston Creek Formation, exposed at the PRC section (~1.3 km north of the eolianite) lies disconformably above the limestone pebble conglomerate (Fig. 2 and 9). The contact between these two is mainly covered, and is thus difficult to find in outcrop. The Ralston Creek is a gypsiferous unit (exposed from 150 m to 158.07 m) composed of gray shale and siltstone beds containing approximately 20–50% pink-orange gypsum nodules (Fig. 10). These are interbedded with medium (> 10 cm thick) gypsum beds, which also contain pink-orange nodules. There are red silica nodules in the upper 2 m of the formation. Thin to thick beds (4–31 cm) of gray, fine-grained sandstone becomes progressively more common starting at 153.42 m. There are three volcanic ash beds in the formation, at 155.4 m, 156.03 m, and 157.23 m, with thicknesses of 9 cm, 6 cm, 1–2 cm, respectively. This formation also contains one 9 cm thick grainstone bed at 157 m. Chert is abundant near the top of the formation. At 157.24 is a 26 cm thick medium sandstone bed with red chert nodules. Ten centimeters above the top of this bed (157.6 m) is a 15 cm thick stromatolite bed with low-relief upward-doming lamination. The bed also contains irregular red chert nodules. A 32 cm thick bed of tan, very fine-grained sandstone bed with blue nodules marks the top of this unit. The strata above the blue

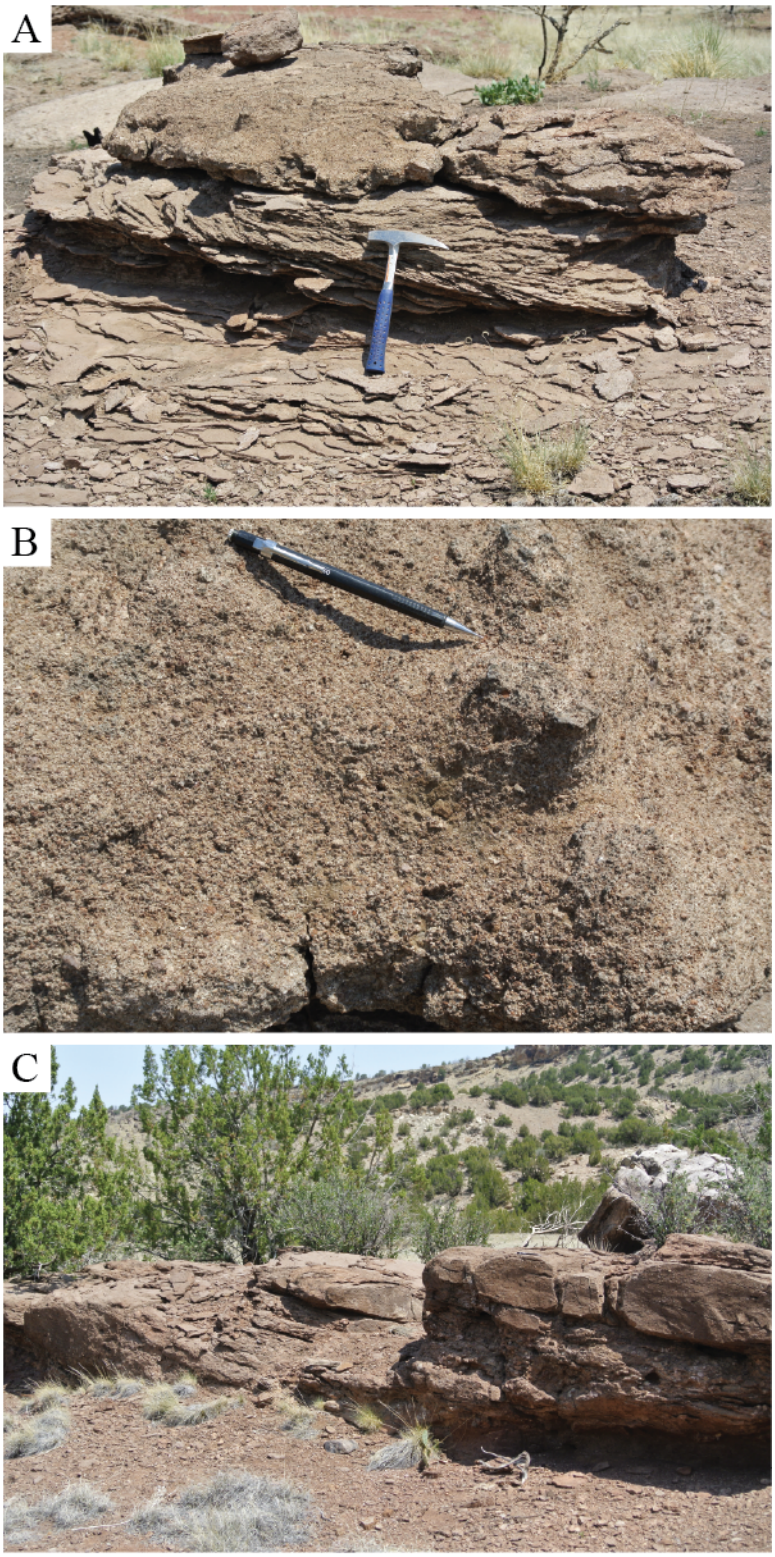

Figure 8: A) Chinle-equivalent unit with trough cross-bedding in the lower bed (hammer is 33 cm long). B) Close-up of pebble conglomeratic texture of the Chinle equivalent. Pencil is 15 cm long. C) Chinle-equivalent strata with coarse pebble conglomerate and overlying pebbly sandstone (unit is ~1 m thick).

Figure 9: PRC Section Stratigraphic Column

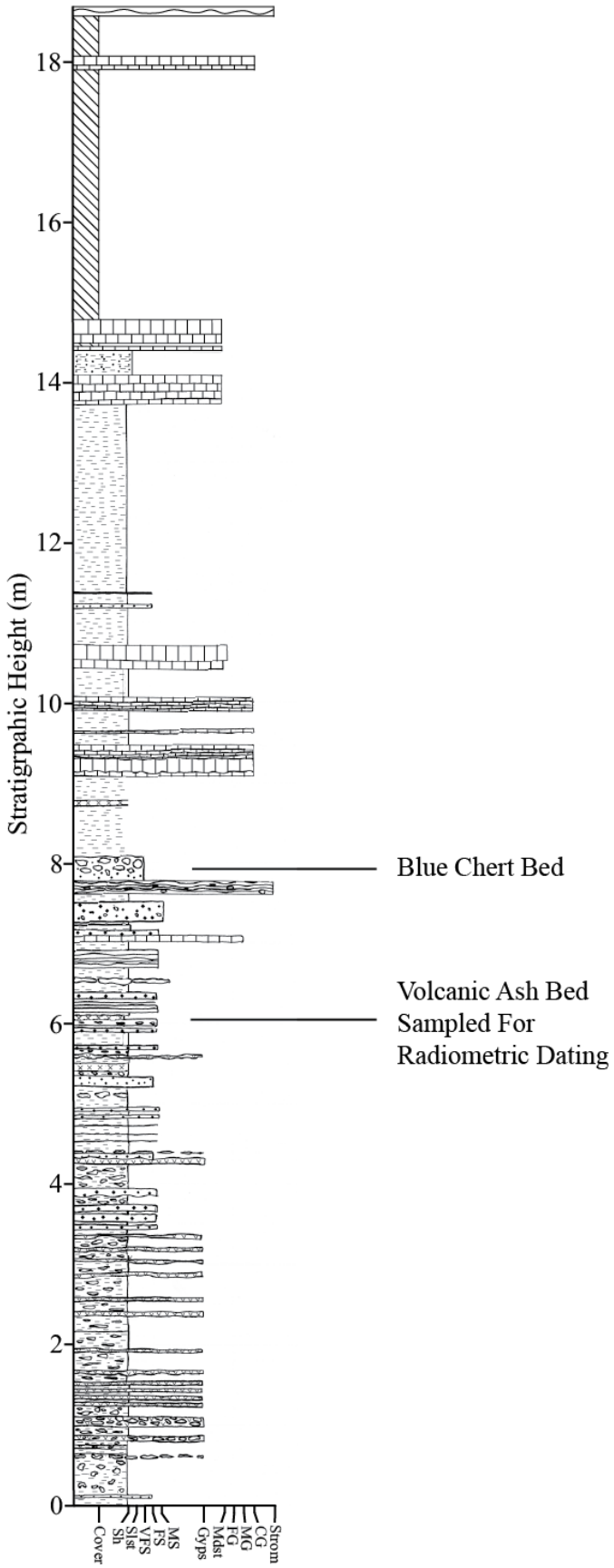

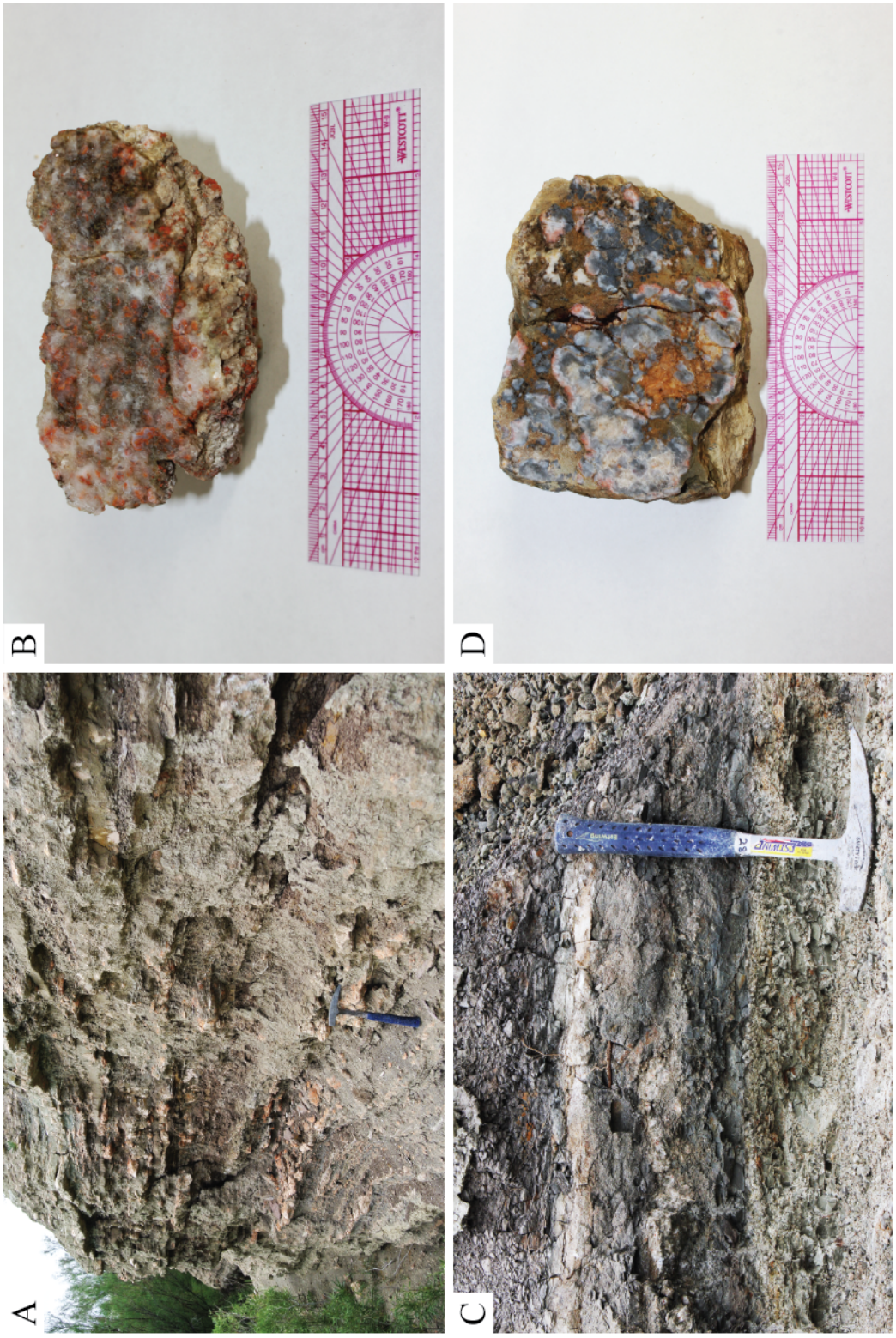

Figure 10: A) Gray gypsum, shale, and siltstone beds with pink-orange gypsum nodules (150 m – 158.07 m). Hammer is 33 cm long. B) Hand sample of gypsum with pink-orange gypsum nodules. Ruler is 15 cm long. C) Green–gray ash bed (bottom bed in picture) located at 155.4 m, which was sampled for U/Pb dating. Hammer is 33 cm long. D) Cut slab of hand sample of the regionally extensive blue chert bed (157.75 m) at top of Ralston Creek Formation. Ruler is 15 cm long.

chert bed, belonging to the lower Morrison Formation, are characterized by alternating thin beds of shale and limestone. From 158.07 m to 159.06 m is 99 cm of dark gray shale, which includes a 15 cm thick volcanic ash bed at 158.7 m. Above the shale unit (9.06 m) is 1.61 m of alternating beds (11–36 cm thick) of gray shale and fine grainstone. The grainstone exhibits wave ripples at 9.06 m and mudcracks at 10.5 m. This is succeeded by 3 m of gray, silty shale with two very thin (2–3 cm thick) beds of fine-grained sandstone at 161.17 m. At 163.67 m there are two units of carbonate mudstone 37 cm and 30 cm thick, separated by a 30 cm thick gray, silty shale bed. The lower mudstone unit has bed breaks of 8–10 cm. Above 164.73 m, there is 2.87 m of cover, followed by a 17 cm bed of oolitic, coarse grainstone (at 167.61 m), and a brown, stromatolitic, coarse grainstone (at 168.11 m).

The upper 3.42 m of the section (from 169.11 m to 172.53 m) is the famous Purgatoire River Dinosaur Trackway site, which exposed at the PFS section ~7 km northwest of the PRC section (Fig. 11). As with the upper PRC section the beds at PFS are part of the Lower Morrison Formation. This unit is predominately composed of alternating beds of gray marlstone and fine-to-medium grainstone (6–45 cm thick), with a 29 cm thick dark gray shale bed at 169.11 m, and 6 cm of medium-grained sandstone at 172.03 m (Fig. 12). Grainstone beds at 169.95 m, 171.4 m, and 172.17 m contain abundant oolites. The exact stratigraphic position of the PFS section relative to the underlying PRC section is undetermined due to cover at this interval. The actual position of the bottom of PFS section is likely within ~1–2 m of the top of the PRC section.

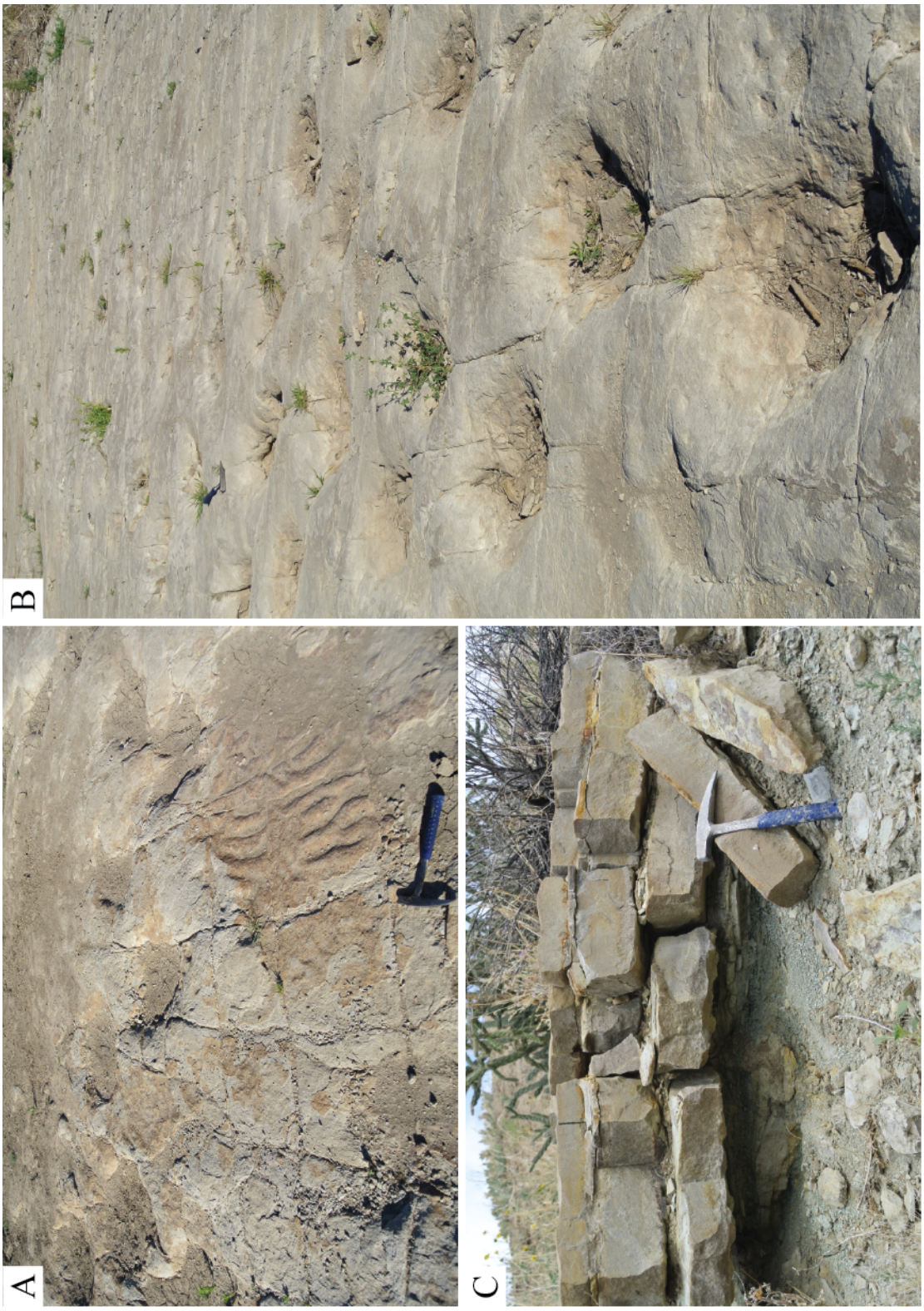

Figure 11: A) Poorly preserved wave ripples adjacent to sauropod tracks. B) Sauropod tracks in oolitic grainstone. Tracks are ~30 cm across. C) Thin to medium beds of oolitic grainstone (above 172.17 m). Hammer for scale is 33 cm long.

Figure 12: PFS Section
Stratigraphic Column

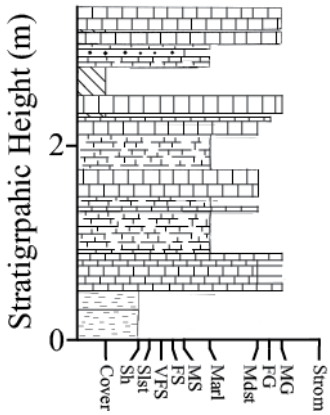

RESULTS

Radiometric U/Pb Dating

Detrital Zircon Dating of BCC mudstone and BCC-2 Eolianite:

$^{206}U/^{238}Pb$ and $^{207}U/^{235}Pb$ dating of 248 zircon grains collected from the BCC-2 section (3 m from its base) yielded a youngest zircon age of 245.5 ± 5.9 Ma (Fig. 13; App. A). The age of this zircon represents the maximum age of the BCC-2 eolianite, which including the error margin is Early Triassic.

Detrital Zircon Dating of BCC Section:

Detrital zircon $^{206}U/^{238}Pb$ dating of the silty mudstone bed at 20.35 m (BCC section) yielded a youngest zircon age of 318.9 ± 1.5 Ma (Middle Pennsylvannian). This was the youngest of four individual zircons grains processed from the sample (App. B).

Volcanic Ash Zircon Dating in the Ralston Creek Formation:

$^{206}U/^{238}Pb$ dating zircon in a Ralston Creek volcanic ash bed located below the blue chert bed (155.4 m) provided an age of 152.987± 0.063 Ma (Kimmeridgian Age). This age is a weighted mean of four out of six individual zircons analyzed (App. C).

Thin Section Analysis of the PFS Oolite:

Thin section analysis of the oolite beds in the PFS section indicates the presence of microbial filaments and mats at the time of deposition. Clotted micrite, or grumeleuse texture, commonly forms the cement surrounding the ooids, and in many cases, also

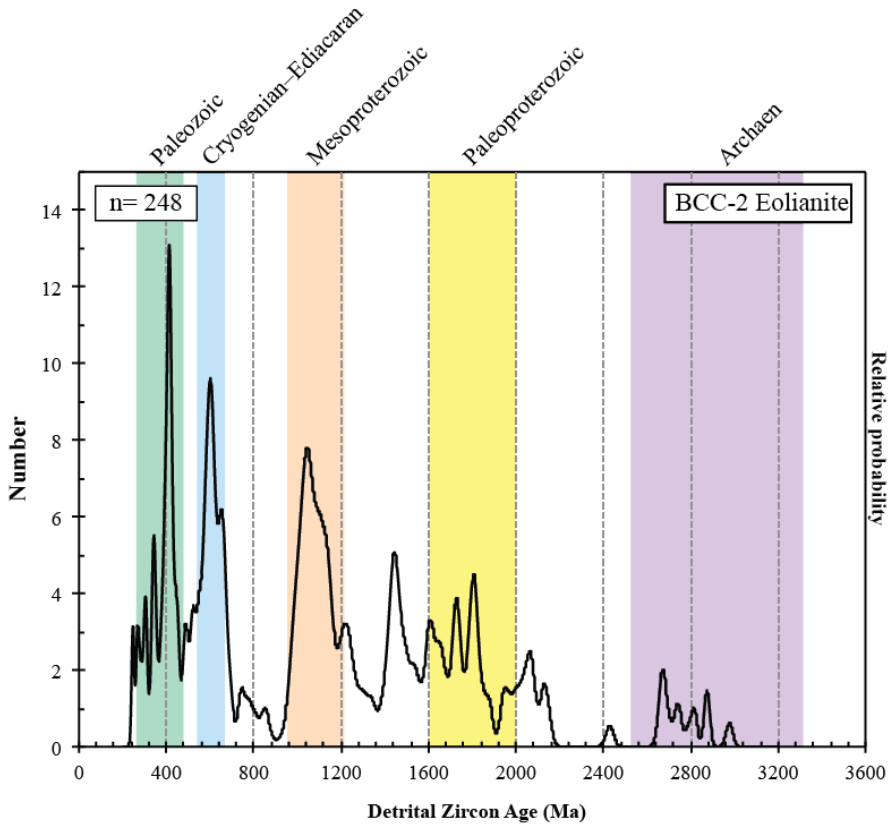

Figure 13: Age spectrum for detrital zircons from the BCC-2 Eolianite

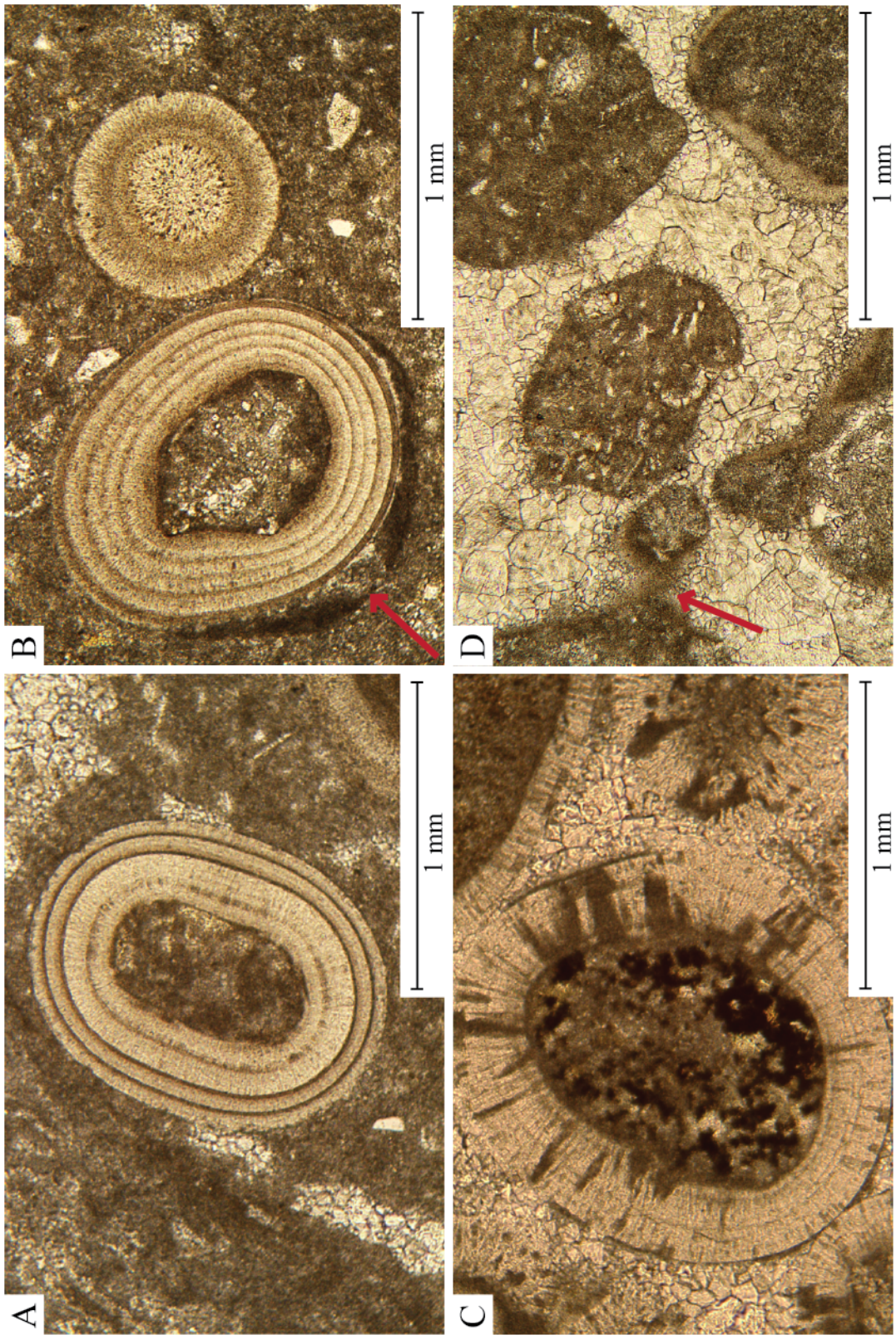

Figure 14: A) Ooid with clotted micrite both surrounding it and within its core. B) Pendant cementation (arrow points pendant). C) Ooid clotted micrite core and radial bore holes. D) Meniscus cementation (arrow points to meniscus).

composes the cores of the ooids (Fig. 14). Micritic cementation of the oolite indicates abundant microbial activity during formation. The presence of the micrite in the cores of the ooids suggests rip-up clasts were torn from the microbial mat in the wave-agitated water. The rip-up clasts were then coated in precipitated calcite, which in the perturbed waters formed ooids. Other rip-up clasts did not form ooids, but are interspersed amongst the ooid clasts. Many of the micrite clasts have micritic envelopes, which are rims around the clasts commonly formed by intense borings of endolithic organisms. Some of the ooids have similar micritic borings forming longate radial "spears" within the cortices.

Micritic cementation between the ooids commonly exists in both meniscate and pendant geometries. Both of these cementation geometries form when the ooids are above the water table. Pendant cementation occurs when a small droplet of water hangs below the ooid through surface tension, thus allowing calcite to precipitate into a meniscus. Similarly, meniscus cementation occurs as water droplet clings to the ooids due to surface tension, but in this case, the droplet forms between two separate ooid grains, and causes precipitation of a calcite meniscus between them. Pendant and meniscus cements are typically formed of clear low-Mg calcite, although those in the PFS ooids are composed of micrite.

Carbonate $\delta^{13}C$ and $\delta^{18}O$ Analysis

BCC Stromatolite and Lykins Formation:

Isotope data of the carbonate in the BCC section can be grouped in two distinct populations (Fig. 15 and 16; App. D), based on their $\delta^{18}O$ and $\delta^{13}C$ values. The first

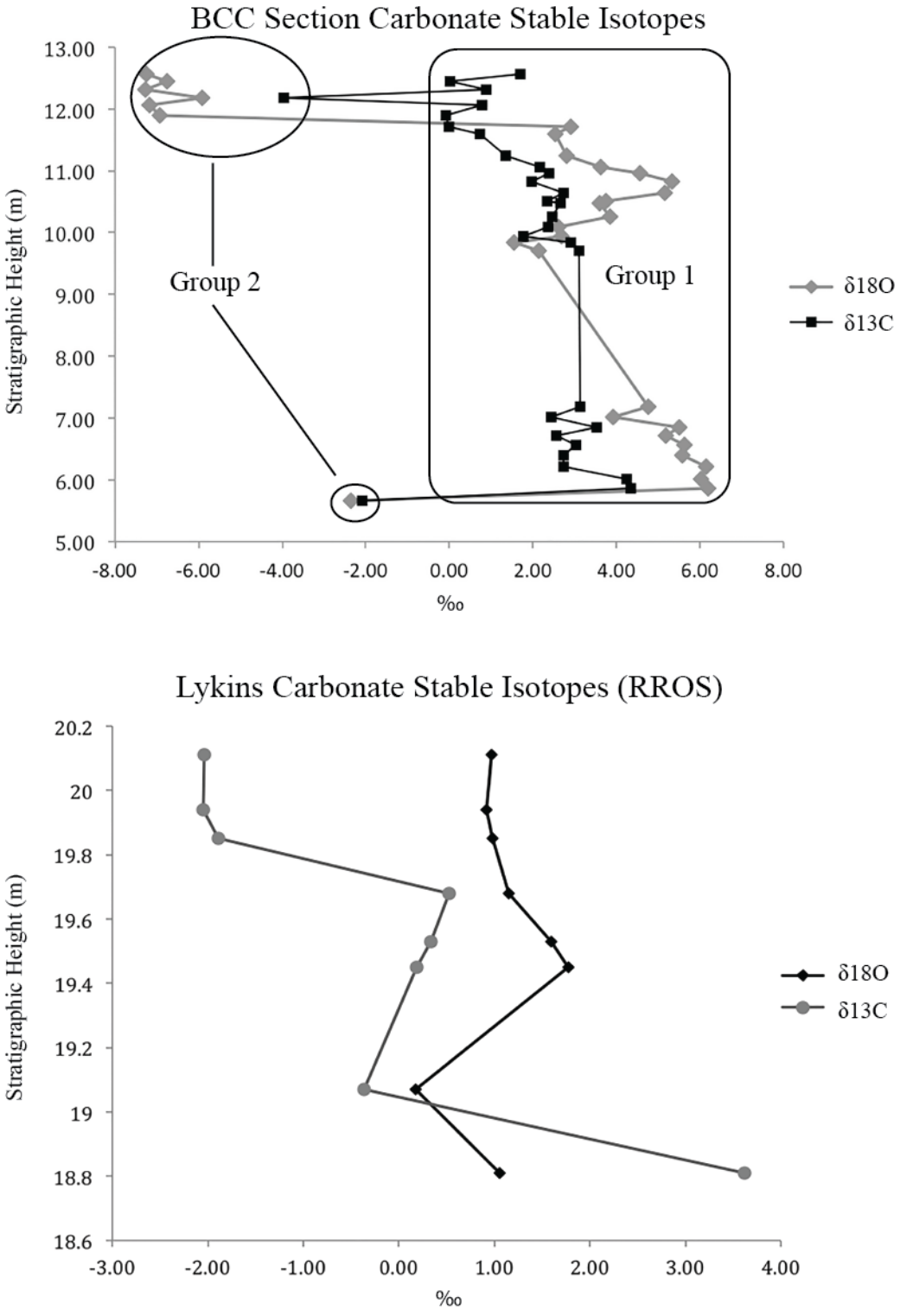

Figure 15: Carbon and oxygen stable isotope δ-values plotted against stratigraphic height. A) Stromatolite at the base of the BCC section. B) Lykins stromatolite at Red Rock Open Space, Colorado Springs, CO

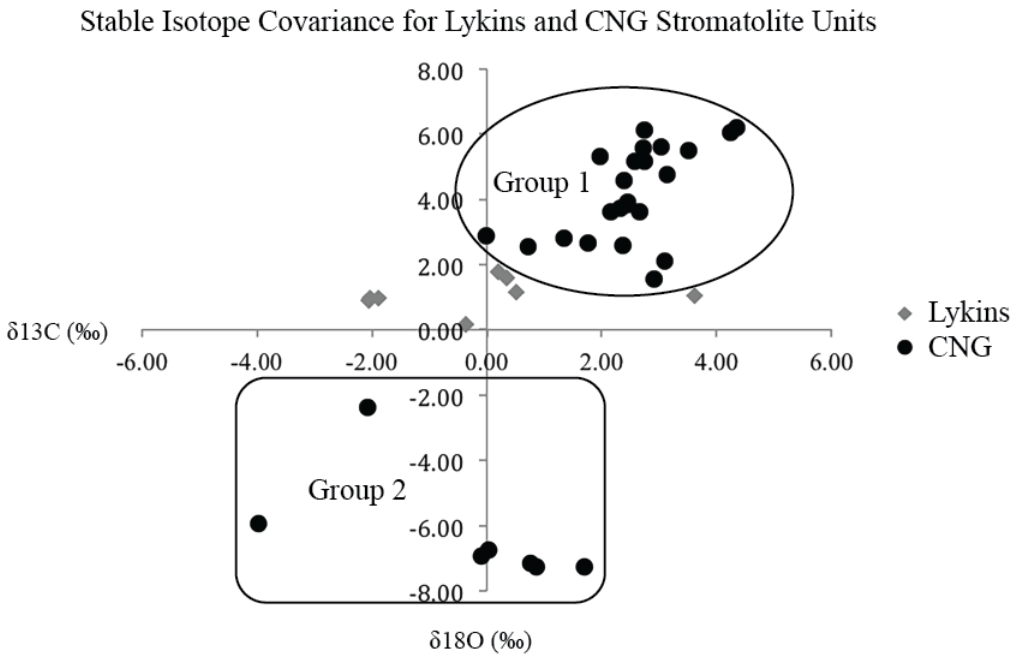

Figure 16: Stable isotope covariance comparison of the stromatolite units at CNG and of the Lykins Formation (measured at Red Rock Open Space, CO). The Lykins Formation stromatolite is characteristic typical marine coastline deposition. The CNG unit contains two distinct groups. The positive group is characteristic of a marine coastline that has been affected by evaporation. The carbon-13 depleted group is too variable to be definitively characteristic of a depositional setting.

population has $\delta^{18}O$ and $\delta^{13}C$ values that range from 1.55‰ to 6.19‰ and –0.02‰ to 4.35‰, respectively. The second BCC isotope data population is scattered and seemingly inconsistent with other data. As these samples were taken from bulk rock, and not from single fossils, it is possible these samples were altered by recrystallization during the dolomitization process.

The carbonate $\delta^{18}O$ and $\delta^{13}C$ values of the stromatolite bed in the Lykins Formation range from –2.05‰ to 3.62‰ and 0.17‰ to 1.77‰, respectively (Fig. 15 and 16; App. D). Values for both $\delta^{18}O$ and $\delta^{13}C$ remain close to 0‰.

Ralston Creek and Lower Morrison Formations:

$\delta^{18}O$ and $\delta^{13}C$ values from carbonate in the Ralston Creek and overlying Lower Morrison members (PRC and PFS sections) are very similar, and coincide with $\delta^{18}O$ and $\delta^{13}C$ carbonate values of the Morrison Formation at Red Rock Open Space (RROS section) in Colorado Springs, CO (Fig. 17 and 18; App. E). Carbonate $\delta^{18}O$ and $\delta^{13}C$ values from the PRC section (both Ralston Creek and lowest Lower Morrison) range from –9.94‰ to –8.09‰ and –6.68‰ to –1.41‰, respectively. The PFS section (Lower Morrison) carbonate values range from –13.09‰ to –5.20‰ and –4.45‰ to –1.42‰, respectively. The $\delta^{18}O$ and $\delta^{13}C$ values for the PFS section have a strong correlation, and have a correlation coefficient of 0.79 if two outliers are removed ([–13.09, 2.95] and [–7.27, –7.03]). Carbonate $\delta^{18}O$ and $\delta^{13}C$ values from the RROS section (Lower Morrison) are similar to the PFS and PRC carbonate, and range from –8.33‰ to –5.98‰ and –4.67‰ to –1.27‰, respectively (Dangles, 2014). All $\delta^{18}O$ and $\delta^{13}C$ values for Morrison

Formation strata are consistent with those presented for the Morrison Formation by Dunagan and Turner (2004).

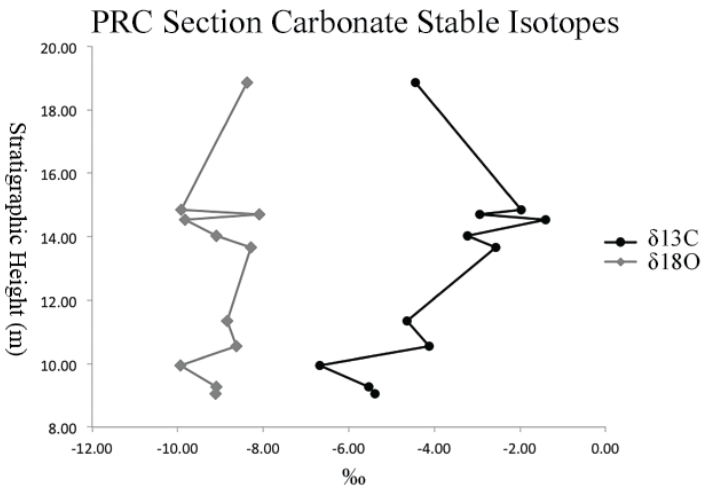

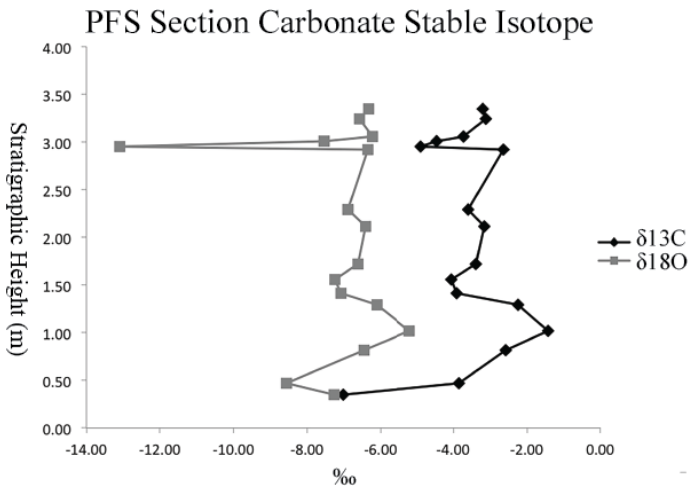

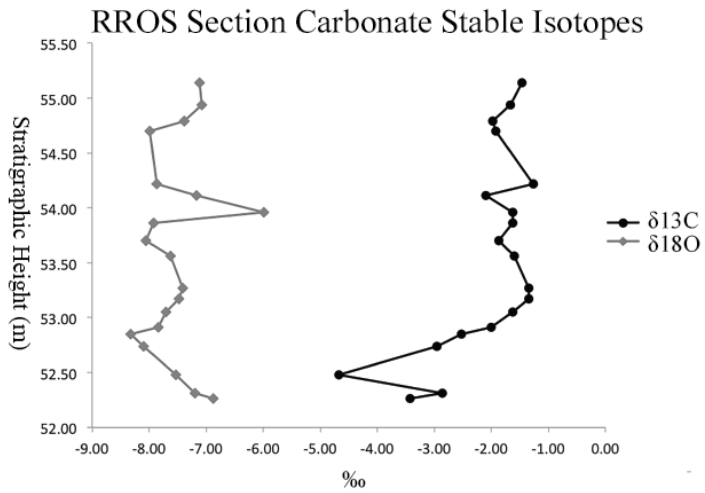

Figure 17: Plots of carbon and oxygen δ-values against stratigraphic height. Graphs show δ-values for PRC and PFS sections, as well as the Morrison Formation measured at Red Rock Open Space (RROS). Negative values for both elements indicates terrestrial deposition.

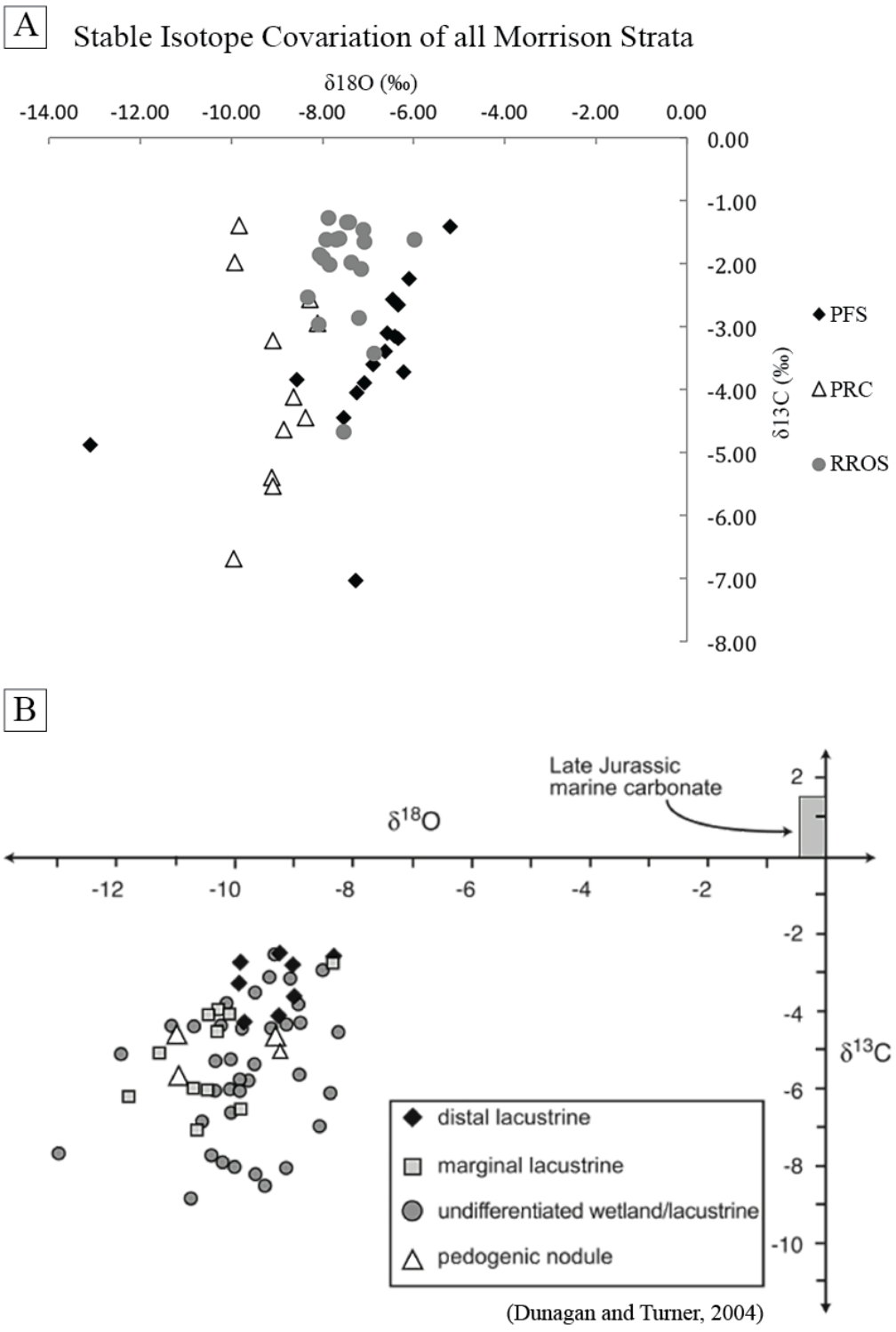

Figure 18: A) Stable isotope covariation plot of all Morrison Formation strata measured in this study. B) Covariation plot of Morrison Formation localities measured by Dunagan and Turner (2004). Note both graphs have very similar distributions.

DISCUSSION

Radiometric Dating

Detrital Zircon Dating of BCC-2 and BCC Sections:

The youngest detrital zircon grain found in the BCC-2 eolianite sample was 245.5 ± 5.9 Ma (Early Triassic), and provides a maximum age constraint for the entire unit, as it was collected from the base of the formation. The Late Triassic fossils in the Chinle conglomerate (Heckert et al., 2012), which disconformably overlies the eolianite, present a minimum age constraint for the eolianite, and when paired with the detrital zircon data, indicate deposition of the BCC-2 eolianite occurred entirely in the Triassic. The data therefore supports the hypothesis of Heckert et al. (2012), which correlates the eolianite to the Red Draw Member of the Jelm Formation (Fig. 19). This designation for the BCC-2 eolianite indicates the southern extent of the Jelm Formation, which at present is in Boulder, CO, needs to be modified to include southeastern Colorado. It is now apparent that Triassic eolian sand dune deposition did not only occur in extensively in Wyoming and northern Colorado, but also locally in southeastern Colorado.

Detrital zircon data from the BCC section (20.35 m) yielded a maximum age constraint of 318.9 ± 1.5 Ma, which is far too old to be an accurate estimate for the strata. While an appropriate age constraint for the BCC section still does not exist, it seems reasonable to correlate the section to the Permian–Triassic Lykins Formation of the Front Range. This is based on the Triassic age of the overlying eolianite, and the lack of any apparent disconformity within the section. Additionally, the Lykins Formation includes strata of both terrestrial and marine deposition, both of which exist in the BCC section. The Forrelle Limestone Member of the Lykins Formation is composed of stromatolitic

Figure 19:
Stratigraphy of Comanche National Grasslands (with age constraints)

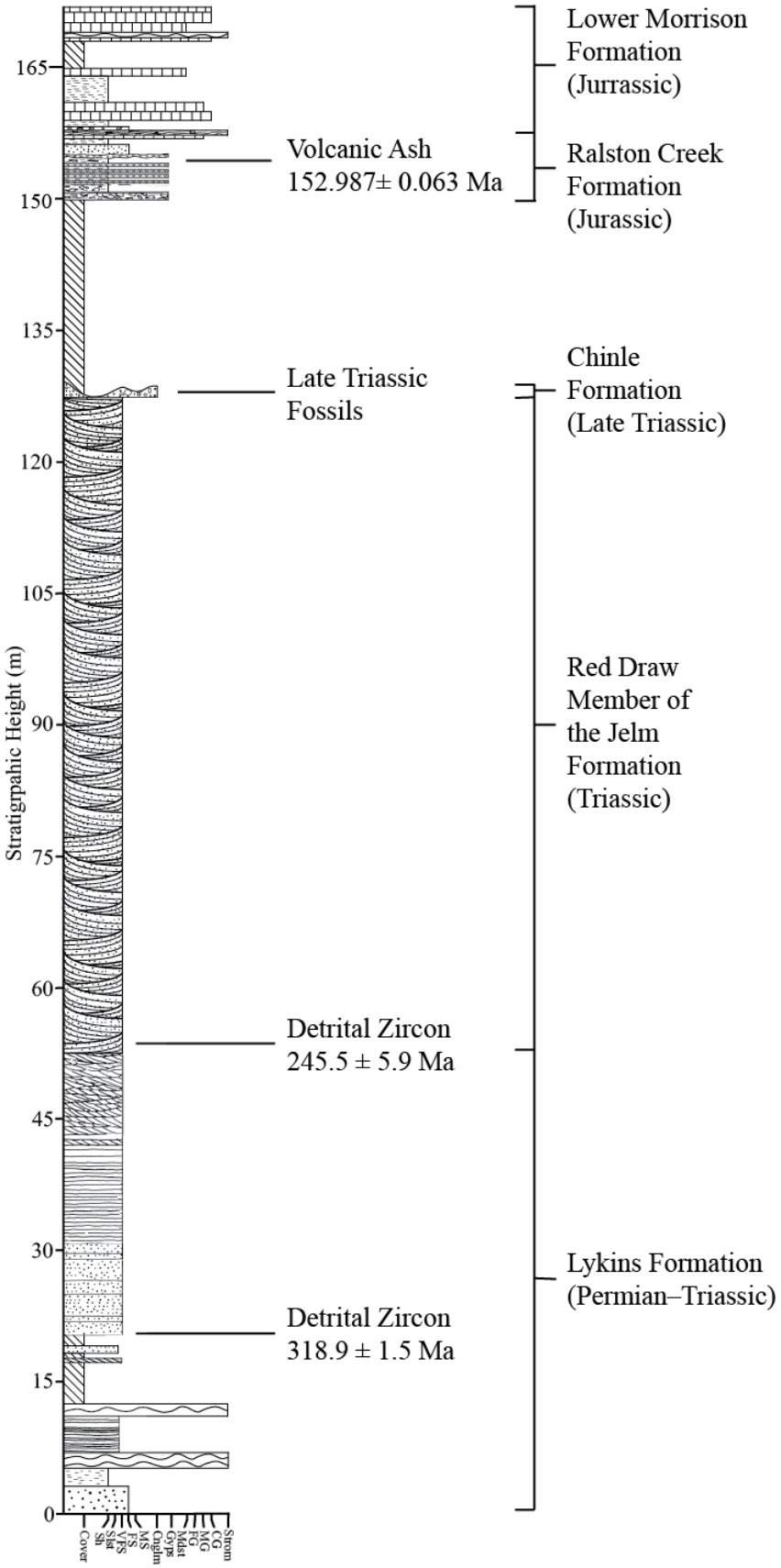

carbonate, and represents the period of prolonged ecological recovery following the P–T extinction. It is likely that the stromatolite beds at the base of the BCC are part of the Forrelle Limestone, and formed as the result of "disaster taxa" becoming prevalent in the general absence of marine predators.

Volcanic Ash Zircon Dating in the Ralston Creek Formation:

U/Pb dating of the volcanic ash bed at 155.4 m yielded an age 152.987± 0.063 Ma, which is the most precise date known for the Ralston Creek or Lower Morrison formations. This indicates the age of the Upper Ralston Creek at CNG is late Kimmeridgian, which is consistent with other Kimmeridigan age approximations for the Ralston Creek (Peterson and Turner, 1998). Kowallis et al. (1998) determine deposition of the entire Morrison Formation occurred over the course of 7 m.y., from 155–148 Ma, based on $^{40}Ar/^{39}Ar$ dating of sanadine and fossil evidence. The age of the Ralston Creek ash bed age is consistent with Kowallis et al. (1998) and other estimates for the Ralston Creek and Morrison formations. This suggests that if the blue chert does indeed represent a disconformity between the Ralston Creek and the Lower Morrison, it was limited in duration.

Thin Section Analysis of the PFS Oolite:

The presence of microbial material, coupled with the unusual cementation geometries in the oolite, have significant implications for its depositional history and the preservation of the dinosaur footprints. Pendant and meniscus cements only form above the water table, where the sediment is unsaturated with respect to water, and individual water droplets can form on grains. Therefore, their presence in the oolite provides evidence of

meteoric vadose diagenesis of the rock. Ooids form in wave-agitated water, and thus the presence of meteoric vadose diagenetic alteration suggest episodes of lower water level and exposure, possibly brought on by increased aridity and evaporation. Episodic exposure would have allowed for the ooid deposits to be above the water table, and for pendant and meniscus cement to form.

The presence micrite both within and between ooid clasts indicates microbes were present pre-, syn-, and post-depositionally. Granular sediment composed primarily of ooids should not by itself be able to preserve footprints, as it lacks cohesive strength and any imprint would quickly collapse. However, it is possible for footprints to be preserved in granular material if microbial mats are present, which can aid in the preservation of footprints. A recent experiment (Marty et al., 2009) investigated this phenomenon by studying the preservation of modern human footprints in sediment incorporating microbial mats. This study states that the primary controls footprints formation and preservation are grain size, yield strength, sediment composition, texture, and rate of sedimentation and erosion. By these guidelines, ooids should not be able to preserve imprints, as the grain size is too great and the yield strength is too little. Nevertheless, Marty et al. (2009) demonstrate that footprints can be preserved in unlikely sediment if microbial mats are present. According to this study, microbes can enhance footprint preservation by dehydration and consolidation of sediment, early diagenic lithification through calcite precipitation, and by binding and stabilizing clasts together, all of which increase cohesion and inhibit imprint collapse. Additionally, the meteoric vadose diagenic cementation exhibited in the oolite would have further increased binding and stabilization of grains. These diagenic changes to the geotechnical behavior of the

sediment would have caused the ooid sediment to alter brittley without subsequent collapse, thus allowing for the unusual taphonomic preservation. Without the presence of microbes and meteoric vadose diagenesis, the world's largest continuously mapped dinosaur trackway would not have formed.

Carbonate $\delta^{13}C$ and $\delta^{18}O$ Analysis

BCC Carbonate and the RROS Lykins Formation:

Positive $\delta^{18}O$ and $\delta^{13}C$ values for both the BCC carbonate and the Lykins Formation at RROS indicate both formed in marine settings. The BCC isotope values are unusual for marine carbonate in that both $\delta^{18}O$ and $\delta^{13}C$ values are more positive than typical marine carbonate. This suggests the carbonate formed in a portion of a coastline that was affected by evaporation. In such a setting, the lighter isotopes of both oxygen and carbon would preferentially evaporate instead of their heavier counterparts, which results in isotopically heavy waters and is reflected in carbonate. It is therefore plausible that the BCC carbonate formed in a tidal flat or coastal lagoon, both which would allow for evaporation and isotopic fractionation of stagnant marine water that is not well mixed with the open ocean. As it now hypothesized that the BCC section does indeed correlate to the Lykins Formation, it is also possible that these unusually high $\delta^{18}O$ and $\delta^{13}C$ values could represent either of the large positive isotopic excursions at the Smithian–Dienerian or Dienerian–Spathian boundaries (Fig. 3). However, the most simplistic interpretation of this data is that it is merely reflective of deposition in evaporation-influenced water.

The $\delta^{18}O$ and $\delta^{13}C$ values of the Lykins carbonate (Forrelle Limestone Member), measured at RROS, are within the expected range of –4‰ to 4‰, and are characteristic

of typical marine deposition. The BCC and RROS stromatolite units likely represent two localities of the same coastline, the first, which formed in a tidal flat or coastal lagoon, and the latter, which formed in the open ocean.

Ralston Creek and Morrison Formations:

The $\delta^{18}O$ and $\delta^{13}C$ values for all Morrison strata overlap with the values of Morrison Formation described by Dunagan and Turner (2004). Negative values for both $\delta^{18}O$ and $\delta^{13}C$ indicate lacustrine deposition. Dunagan and Turner (2004) characterize Morrison lacustrine deposits to have formed in hydraulically open basins on the basis that $\delta^{18}O$ and $\delta^{13}C$ values are not strongly correlated. This would suggest water is escaping the basins by means other than evaporation. In such an environment, carbonate isotope ratios mostly reflect the composition of water input, and is not largely affected by evaporative isotopic fractionation. $\delta^{18}O$ and $\delta^{13}C$ data from the PRC and RROS carbonate are not correlated and support Dunagan and Turner's hypothesis. The PFS section is unusual in that carbonate $\delta^{18}O$ and $\delta^{13}C$ values from the PFS section do show a moderate correlation ($r = 0.53$). With the exception of two data points ([–13.09, 2.95] and [–7.27, –7.03]), the data PFS covariation plot depicts a well-defined, positive correlation. In fact, if the two outliers are removed, the correlation coefficient for the rest of the PFS data increases to 0.79. This is a significantly stronger correlation than the $r = 0.1–0.5$ range established by Dunagan and Turner (2004) for the Morrison Formation.

Talbot (1990) states lacustrine carbonate with a correlation coefficient of > 0.70 are indicative of deposition in a hydraulically closed system where water output from the basin primarily occurs through evaporation. This results in isotopic fractionation of the

water where heavier isotopes remaining in a liquid state, while the lighter isotopes are evaporated. This process can occur with both oxygen and carbon, with oxygen primarily evaporating as gaseous H_2O and carbon evaporating as CO_2 (Dunagan and Turner, 2004; Talbot, 1990). Isotope values re-equilibrate during periods of less evaporation and more water input. Correlated $\delta^{18}O$ and $\delta^{13}C$ values can therefore be used as a proxy to qualify relative aridity, as a strong correlation reflects evaporation.

As stated previously, thin sections of the PFS oolite beds indicate calcite precipitation and cementation above the water table. It is hypothesized, therefore, that a similar process to that of hydraulically closed systems outlined by Talbot (1990) occurred during of the cementation PFS oolite, except that in this case, isotopic correlation is because of evaporation of pore water, and not of lake water. Although changes in aridity are apparent in the lithology throughout the PRC, RROS, and PFS section, isotopic correlation is only prevalent in the PFS section, where vadose calcite precipitation is evident. Periodic fluctuations in aridity allowed for the precipitation of calcite and micrite between ooid clasts because of pore water evaporation. As a result, this increased the overall cohesive strength of the sediment to a point at which imprints could be preserved. The preservation of the dinosaur footprints is, therefore, largely due to the fluctuations in aridity during deposition.

Such pronounced correlation between $\delta^{18}O$ and $\delta^{13}C$ values does not occur in the PRC or RROS carbonate, and it is possible that the strong correlation is the result of diagenesis. However, because periodic increases in aridity and evaporation are evident in the depositional facies regionally throughout the Morrison Formation, it seems likely that

the isotopic signature of the PFS carbonate accurately reflects changes in aridity, and is not diagenically altered.

FACIES INTERPRETATION

The base of the BCC section (< 12.58 m) is characteristic of marine coastline deposition. The thinly laminated, parallel beds of claystone, siltstone, and very fine-grained sandstone are indicative of deposition from suspension in water. The stromatolite beds from 5.67–7.07 m and 11.07–12.58 m indicate formation in shallow water, as stromatolites require sunlight to grow. As noted previously, the $\delta^{18}O$ to $\delta^{13}C$ values of the stromatolite beds suggest the stromatolites formed in a coastline environment affected by evaporation. This could be either a tidal flat or marine coastline lagoon. If these beds did in fact form in a tidal flat, it would be expected that sedimentological structures associated with tidal flats, such as mudcracks or stoss-preserving dunes and ripples, exist in proximity within the section, which they do not. Instead, the low energy deposition of the surrounding claystone, siltstone, and very fine-grained sandstone beds supports the converse hypothesis that deposition occurred in a coastline lagoon, not in a tidal flat. Again, the stromatolite unit is likely part of the Forrelle Member of the Lykins Formation, and is representative of "disaster taxa" succeeding the P–T mass extinction.

The strata between the stromatolite and the eolianite units, from 12.58–50.21 m at BCC, indicates a transition from marine to terrestrial deposition, and reflects a relative marine regression. Small symmetrical ripples (at 13.70 m) suggest traction transport under waves in a shallow water environment, and could record the transition period of the regression. These ripples are immediately succeeded by mudcracks (13.75 m), which mark the initiation of terrestrial deposition. Current ripple cross-lamination (at 13.89 m, 34.35 m and 40.48 m) and dune-scale cross-stratification (at 32.03 m and 32.69 m) indicate deposition under unidirectional flow, typical of fluvial deposits. Cross-bed sets

up to 50 cm thick suggests reasonably strong stream currents, and water depths of at least 2–3 m (Yalin, 1964; Gabel, 1993). The well-sorted, fine grain size of all of the units (shale, siltstone, very fine to fine-grained sandstone) in this section indicates deposition was distal from areas of high topographic relief. Massive, fine-grained sandstone and siltstone beds throughout this section suggest deposition also occurred through sediment precipitation from suspension in water. The massive beds are therefore interpreted as floodplain or lacustrine deposits, which alternate with fluvial deposits with channel migration. Mudcracks throughout the section (13.70 m, 13.96 m, 27.83 m and 43.15 m) support this interpretation, and represent drying of floodplains or lakes. Mudcracks also suggest an arid climate at this time.

All of the units from 0–50.21 m are red, purple, or orange, and are members of the Pennsylvanian–Triassic 'red beds' of the southwestern United States. Red coloration in strata occurs on a spectrum from red to purple to green that is based on the ratio of Fe^{3+}/Fe^{3+} in clasts (Myrow, 1990). The Fe^{3+}/Fe^{2+} ratio in detrital grains dictates the type of iron oxide that is created in early post-depositional reactions, and subsequently controls where color falls on the spectrum (Myrow, 1990). This process is dependent on iron reduction and oxygenation (redox) reactions, as influenced by the surrounding environment. In anoxic environments iron is reduced to the soluble Fe^{2+} ion, which is then flushed out of the system by the reducing fluid. In this case, the rock will be bleached white, as all iron has been removed. Conversely, in near surface environments, iron is oxygenated to insoluble Fe^{3+}, which forms iron oxide and gives the rock a red, orange, or purple color. The coloration of the rock occurs on a spectrum depending on the degree of oxygenation and reduction, in which white and green are indicative of reducing

environment, red and purple is indicative of hematite and highly oxygenated environments, and orange is a middle member (usually formed by goethite). Color intensity may also be influenced by detrital grain size, as small grains allow for higher iron content by surface area (Myrow, 1990). Intense red, purple, or orange coloration is characteristic of Laurentian Pennsylvanian to Triassic strata of the southwest, which are composed of sediment eroded from the Ancestral Rocky Mountains, and deposited in dominantly terrestrial settings. These strata are rich in iron oxide, and are characteristic of well-oxygenated depositional and post-depositional environments.

The 77 m thick eolianite unit at 50.21 m indicates a transition in paleoenvironments from a fluvial system into a persistent sand dune field. The maximum age of this unit of 245.5 ± 5.9 Ma, as determined by radiometric dating of detrital zircons, indicates deposition occurred in the Triassic, and that this unit is part of the Red Draw Member of the Jelm Formation. The existence of a supersurface (a regionally extensive, flat surface that truncates a dune sequence) in the upper part of the eolianite provides evidence for a hiatus in erg (dune field) deposition. Supersurfaces were originally interpreted as surfaces where the groundwater table elevated to the top of the dune field (Stoke, 1968). As wind does not have much of an effect on transporting saturated sand, the overlying layer of dry sand erodes away while the saturated sand remains in place, thus creating a non-depositional surface on top of the groundwater table. Supersurfaces may also form during a hiatus in deposition when the area is temporarily abandoned by migrating dunes and briefly becomes a non-depositional environment (Kocurek, 1988). It is also possible this supersurface is a result of a temporary shift to a more humid climate that could have increased plant abundance and decreased sand mobility (Kocurek, 1988).

Secondary oxidation processes outlined above for the BCC section may have caused the red color of the eolianite; however, it is also plausible the coloration is a result of primary oxidation processes taken place during deposition. Syn-depositional oxidation of grains in eolian deposits is dependent on the transport distance of grains, the iron content of the parent rock, and the presence of both atmospheric water content and groundwater (Walker, 1979). Modern sand dunes in western Libya show an increase in red coloration with increased transportation distance (Walker, 1979). Similarly, a high iron content in the parent rock or increased humidity can cause syn-depositional oxidation. If the red coloration of the eolianite is syn-depositional, it could therefore indicate extensive transport distance or a mildly humid climate.

The Chinle pebble conglomerate lies disconformably above the Jelm Formation (at 127 m), and is interpreted as a fluvial deposit because of its lenticular beds, trough cross-bedding, and rounded fossils. The extent of the hiatus between the Jelm and the Chinle formations is undetermined, however, it was likely short-lived, as Triassic strata exist on either side on the disconformity. The stream channels of the Chinle Formation were fairly distal to the source rock, as no clasts exist larger than pebble-size. Stream channels had moderately strong currents to transport coarse material. The fossils in the Chinle conglomerate are likely from the Carnian Stage of the Upper Triassic, and best correlate to the lower Chinle Formation (Heckert et al., 2012). The fossils are rounded and abraded, suggesting they had been transported prior to deposition.

The J–5 Unconformity is regionally at the base of the Upper Jurassic Ralston Creek Formation (Peterson and Turner, 1998), and is located at the Chinle–Ralston Creek contact at CNG. The Ralston Creek Formation is dominated by mudstone and fine-

grained sandstone north of Denver, CO, but it transitions into a prevailing gypsiferous facies in southern Colorado (Peterson and Turner, 1998). The Ralston Creek Formation in CNG is dominated by gypsiferous shale, siltstone, and fine-grained, which is indicative of deposition from suspension in low-energy waters, likely in a shallow, lacustrine setting. Alternating gypsiferous beds indicate periods of hypersalinity and alkalinity in very shallow water, which then episodically freshened with input of fresh water. This cycle is indicative of periodic changes in aridity leading to fluctuations in evaporation rate.

As with the color spectrum of iron bearing sediment, a spectrum exists for shale with light gray to black coloration that is dependent on preservation of organic material. The shade of gray in shale is principally dependent on availability of organic carbon and of oxygen used in oxidation reactions (Myrow, 1990). Unlike the iron oxidation and reduction, organic oxidation cannot be reversed; thus, the shade of organic shale can be used as a paleoenvironmental indicator. The shale and siltstone of the Ralston Creek Formation at the PRC section is light gray, and is indicative of an oxygenated environment. The lighter coloration of the strata either indicates a limited amount of organic material, or that the organic material was only partially oxygenated.

The blue chert layer (at 157.75 m), also described as the ‘welded chert’ bed (Ogden, 1954), is a regionally pervasive unit with a variety of colors, and is occasionally used as a crude stratigraphic marker for the contact between the Ralston Creek and Morrison formations (Lockley et al., 1986). Although the two formations are lithologically similar, and interfinger locally, near Denver, CO (Peterson and Turner, 1998), it is possible the blue chert bed represents a hiatus in deposition at CNG. The blue chert layer is a

terrestrial silcrete, of which little is known about its formation. There are two hypotheses as to how it may have formed: (1) post-burial dissolution by groundwater, and eventual precipitation of silica derived from the diagenesis of surrounding volcanic ash beds (King and Merriam, 1969); and (2) pedogenic silcrete formed as part of a subaerial, soil-weathering reaction. Pedogenic chert is produced in a weathering process in which silica is dissolved from a source rock and infiltrates the soil via illuviation (Simon-Coinçon, 1996). Pedogenic chert is typically correlated with a shift to a more arid climate, as increased aridity also increases evaporation rate, which subsequently causes precipitation and a recrystallization of the dissolved silica (Simon-Coinçon et al., 1996). As with the first hypothesis, likely sources of silica for this reaction are the volcanic ash of this succession. If the blue chert bed is in fact a pedogenic silcrete, it could represent a hiatus in deposition during which the bed was directly under a subaerial exposure surface. However, radiometric dating an underlying ash bed in the Ralston Creek Formation is similar to previous dates for the Morrison Formation, suggesting such a hiatus in deposition would have been short lived.

The strata above the blue chert bed (> 158.09 m) at the PRC section and the strata at the PFS section are correlated to the Lower Morrison Formation (Lockley et al., 1986; Kowallis et al., 1998; and others), which is considered to consist of primarily lacustrine deposits formed in a basin that spanned northern New Mexico, Oklahoma, Kansas, and southeastern Colorado (Lockley et al., 1986; Kowallis et al., 1998; Dunagan and Turner, 2004). The strata consist of light gray to dark gray shale and siltstone beds alternating with marlstone and oolitic grainstone. Lockley et al. (1986) describes these facies as shallow lacustrine shale deposits alternating with shoreline carbonate deposits, as

determined by fluctuations of water. It is also possible that the alternating facies is a consequence of climatically controlled oscillations of siliciclastic sediment input into the lake, which killed carbonate-forming organisms during excessive influxes of sediment.

Lockley et al. (1986) is an extensive interpretation of the paleoenvironmental conditions of the lower Morrison Formation that uses fossil and sedimentary evidence. Wave ripples are pervasive throughout the Lower Morrison in southeastern Colorado, indicating a regionally shallow lake environment. Additionally, Lockley et al. (1986) report the existence of *Chara* fossils (freshwater green algae), which do not live in water deeper than 3 m. Oolitic grainstone is common throughout the Lower Morrison, and signifies wave agitation in very shallow water settings.

The Lockley et al. (1986) interpret well-oxygenated shallow water environments for the Lower Morrison on the basis of the gray color of the shale, which may suggest only moderate preservation of organic matter. However, some shale beds are dark gray, indicating a fairly high preservation rate. Sedimentation rate has complex effects of organic redox reactions. An increase in sedimentation rate causes rapid burial of organic carbon, which would intuitively increase organic preservation rate (Myrow, 1990). However, increased sedimentation rates can also generate an increase in microbial decomposition of organic carbon, thus decreasing total organic carbon preservation (Myrow, 1990; Berner 1978). It therefore seems likely that the basin either went through periods of anoxic or dysaerobic water that episodically inhibited organic decomposition, or was subject to fluctuations of fluvial sediment input that had complex and varying effects on the decomposition of organics.

Stromatolites outcrop at the PRC section, as well as regionally within the Morrison Formation (Neuhausser et al., 1987), and suggest periods of saline waters, which likely correspond intervals of increased aridity and evaporation. This is further supported by salt-casts found on the basal contact of some impermeable sandstone beds (Lockley et al., 1986). Such fluctuations in aridity and evaporation are evident throughout the Ralston Creek and Lower Morrison formations in lithology, thin section, and stable isotope analysis. As previously discussed, alternating gypsum beds in the Ralston Creek formation, strong correlation between $\delta^{18}O$ and $\delta^{13}C$ values in the PFS section, and meteoric vadose diagenesis are all indicative of oscillations in aridity and evaporation. Deposition of the Morrison Formation is considered to have occurred in primarily hydraulically open basins, as indicated by the general lack of correlation between $\delta^{18}O$ and $\delta^{13}C$ values (the PFS section excluded; Dunagan and Turner, 2004). Fluvial input is typically considered to be the primary process in which lakes in open basins are maintained; however, sufficient fluvial flow to refill basins would not be possible in such an arid climate. Dunagan and Turner (2004) suggest the lakes of the Morrison Formation were, in fact, groundwater fed, and not the product of fluvial input. This seems to be the most accurate interpretation of the paleoclimate of the Morrison Formation.

CONCLUSION

This study has developed a complete Early Mesozoic stratigraphy for Comanche National Grasslands, established ages for the oldest strata, and explained an odd taphonomic occurrence. The oldest strata in Picket Wire Canyon, which were previously of undetermined age, are now known to be latest Permian–Triassic. The Lykins Formation constitutes the oldest strata at CNG, and is composed of marine carbonate, which transitions into fluvial deposits following a marine regression. Red Draw Member of the Jelm Formation succeeds the Lykins Formation, and marks a transition to eolian deposition. The thin Chinle Formation disconformably overlies the Jelm Formation, and represents the final phase of Triassic deposition at this locality. The Jurassic strata, consisting of both the Ralston Creek and Morrison formations, represent lacustrine deposition in a fluctuating arid climate. The blue silcrete bed at the contact of these formations, either does not represent a disconformity, or represents only a short-lived hiatus in deposition. Additionally, microscopic evidence indicates preservation the famous CNG dinosaur footprints is principally the result of microbial activity, which bound and stabilized clasts by dehydration and consolidation of sediment, as well as early diagenic cementation.

Although the correlation of the BCC section to the Lykins Formation seems to be a logical assumption, additional research is necessary to empirically supports this designation. Perhaps the most promising approach for this would be the use of strontium isotope chemostratigraphy of the BCC stromatolite section. Correlating strata to other formations using only carbon isotope chemostratigraphy can be challenging, as carbon isotope fluctuations can be extremely rapid, especially following the P–T extinction.

Strontium isotope chemostratigraphy when used in conjunction with carbon isotopes can therefore be a powerful tool, as strontium isotope ratios are ultimately controlled by tectonism and thus oscillate on considerably larger timescales than carbon isotope ratios (Joachimski et al., 2012). In order for this approach to be effective in the BCC stromatolite with other regional formation, samples for strontium and carbon isotope analysis should also be collected from the Forelle Member of the Lykins Formation to serve as a comparison. Hopefully, this approach would lead to an accurate chemostratigraphic correlation to a known regional formation, which in doing so would constrain the age of the BCC stromatolite, and provide a better age approximation for the strata.

REFERENCES

Berner, R.A., 1971, Principles of chemical sedimentology: McGill-Hill Book Company, New York, p. 240

Clayton, R.N., and Degens, E.T., 1958, Use of carbon isotope analyses of carbonates for differentiating fresh-water and marine sediments, AAPG Bulletin, v. 43, no. 4, p. 890-897

Corsetti, F.A., Baud, A., Marenco, P.J., and Richoz, S., 2005, Summary of Early Triassic carbon isotope records: Comptes Rendus Palevol, v. 4, p. 473–486

Cragin, F. W., 1896, The Permian System in Kansas: Colorado College Studies, v. 6, p. 1-48.

Craig, H., 1953, the Geochemistry of the stable carbon isotopes: Geochimica et Cosmochimica Acta, v. 3, p. 53

Dangles, L., 2014, Triassic–Jurassic strata of the Colorado Springs region and associated palynoflora [Senior Project]: Colorado College

Dickins, A.P., 1995, Radiogenic Isotope Geology: Cambridge University Press, Cambridge; New York

Dickinson, W.R., and Gehrels, G.E., 2003, U–Pb ages of detrital zircons from Permian and Jurassic eolian sandstones of the Colorado Plateau, USA: Paleogeographic implications: Sedimentary Geology, v. 163, p. 29–66

Dickinson, W.R., and Gehrels, G.E., 2010, Implications of U–Pb ages of detrital zircons in the Mesozoic strata of the Four Corners Region for the provenance relations in space and time: New Mexico Geological Society Guidebook, 61st Field Conference, Four Corners Country, p. 135-146

Dunagan, S.P., and Turner, C.E., 2004, Regional paleohydrologic and paleoclimatic settings of wetland/lacustrine depositional systems in the Morrison Formation (Upper Jurassic), Western Interior, USA: Sedimentary Geology, v. 167, p. 269–296

Faure, G., 1998, Principles and Applications of Geochemistry, Second Edition: New Jersey, Prentice Hall Inc.

Gabel, S.L., 1992, Geometry and kinematics of dunes during steady and unsteady flows in the Calamus River, Nebraska, USA: Sedimentology, v. 40, p. 237–269

Galfetti, T., Buchar, H., Brayard, A., Hochuli, P., Weissert, H., Guodon, K., Atudorei, V., Guex, J., 2007, Late Early Triassic climate change: Insights from carbonate carbon isotopse, sedimentary evolution and ammonoid paleobiogeography: Palaeogeography, Palaeoclimatology, Palaeoecology, v. 243, p. 394–411

Gehrels, G., and Pecha, M., 2014, Detrital zircon U–Pb geochronology and Hf isotope geochemistry of Paleozoic and Triassic passive margin strata of western North America: Geosphere, v. 10, no. 1, p. 49–65, doi: 10.1130/GES00889.1

Heckert, A.B., Sload, E.J., Lucas, S.G., and Schumacher, B.A., 2012, Triassic fossils found stratigraphically above ‘Jurassic’ eolianites necessitate the revision of lower Mesozoic stratigraphy in Picket Wire Canyonlands, south-central Colorado: Rocky Mountain Geology, v. 47, no. 1, p. 37–52

Joachimski, M.M., Lai, X., Shen, S., Jiang, H., Lou, G., Chen, B., Sun, J.C., and Sun, Y., 2012, Climate warming in the latest Permian and the Permian–Triassic mass extinction: Geology, v. 40, p. 195–198, doi: 10.1130/G32707.1

Keith, M.L., Anderson, G.M., and Eichler, R., 1964, Carbons and oxygen isotopic composition of mollusk shells from marine and fresh-water environments: Geochimica et Cosmochimica Acta, v. 28, p. 1757–1786

Keith, M.L., and Weber, J.N., 1964, Carbon and oxygen isotopic composition of selected limestones and fossils: Geochimica et Cosmochimica Acta, v. 28, p. 1787–1816

King, R., and Merriam, D., 1969, Origin of the "Welded Chert," Morrison Formation (Jurassic), Colorado: Geological Society of America Bulletin, v. 80, no. 6, p. 1141–1148

Kocurek, G., 1988, First-order and super bounding surfaces in eolian sequences–Bounding surfaces revisited: Sedimentary Geology, v. 56, p. 193–206

Korte, C., and Kozur, H.W., 2010, Carbon-isotope stratigraphy across the Permian–Triassic boundary: A review: Journal of Asian Earth Sciences, v. 39, p. 215–235

Kowallis, B.J., Christiansen, E.H., Deino, A.L., Peterson, R., Turner, C., Kunk, M., and Obradovich, J., 1998, The age of the Morrison Formation: Modern Geology, v. 22, p. 235–260

Kump, L.R., 1987, Alternative modeling approaches to the geochemical cycles of carbon, sulfur, and strontium isotopes: American Journal of Science, v. 289, p. 390–410

Link P.K., Mahon R.C., Beranek, L. P., Campbell-Stone, E.A., and Lynds, R., 2014, Detrital zircon provenance of Pennsylvanian to Permain sandstones from the Wyoming craton and Wood River Basin, Idaho, USA: Rocky Mountain Geology, v. 49, n. 2, p. 115–136

Lockley, M.G., Houck, K.J., and Prince, N.K., 1986, North America's largest dinosaur trackway site: Implications for the Morrison Formation paleoecology: Geological Society of America Bulletin, v. 97, no. 10, p. 1163–1176

Marty, D., Strasser, A., and Meyer, C., 2009, Formation and taphonomy of human footprints in microbial mats of present-day tidal-flat environments: implications for the study of fossil footprints: Ichnos, v. 16, p. 127–142

Maslin, M. A., Swann, G.E.A., 2006, Isotopes in marine sediments, *in* Leng, M. J., ed., Isotopes in Palaeoenvironmental Research: Springer Netherlands, p. 227–290, doi: 10.1007/1-4020-2504-1_06

Maughan, E. K., 1980, Permian and Lower Triassic geology of Colorado, *in* Kent, H. C., and Potter, K. W., eds., Symposium on Colorado geology, Rocky Mountain Association of Geologists Geological Conference Guidebook, p. 103–110.

McKee, E. D., et al., 1956, Paleotectonic maps of the Jurassic system: Washington, D.C., U.S. Geological Survey, Miscellaneous Geologic Investigations Map I-175, 6p.

Myrow, P.M., 1990, A new graph for the understanding colors of mudcracks and shales: Journal of Geological Education, v. 38, p. 16

Neuhauser, K., Lucas, S., Albuquerque S., Louden, R., Hayden, S., Kietzke, K., Oakes, W., Marais, D., 1987, Stromatolites of the Morrison Formation (Upper Jurassic), Union Country, New Mexico: a preliminary report: New Mexico Geological Society Guidebook, 38th Field Conference, Northeastern New Mexico, p. 153–160

Ogden, L., 1954, Rocky Mountain Jurassic time surface: American Association of Petroleum Geologists Bulletin, v. 38, no. 5, p. 914–916

Peterson, F., and Turner, C., 1998, Stratigraphy of the Ralston Creek and Morrison Formations (Upper Jurassic) near Denver, Colorado: Modern Geology, v. 22, no. 1–4

Richter, F.M., Rowley, D.B., and DePaolo, D.J., 1992, Sr isotope evolution of seawater: the role of tectonics: Earth and Planetary Science Letters, v. 109, p. 11–23

Saltzman, M.R., and Sedlacek, A.R.C., 2013, Chemostratigraphy indicates a relatively complete Late Permian to Early Triassic sequence in the Western United States: Geology, v. 41, p. 399–402, doi: 10.1130/G33906.1

Schubert, J.K., Bottjer, D.J., 1992, Early Triassic stromatolites as post-mass extinction disaster forms, Geology, v. 20, p. 883-886, doi: 10.1130/0091-7613(1992)020<0883:ESTSAPM>2.3.CO;2

Schumacher, 2010, personal communication, December, 2014

Simon–Cinçon, R., Milnes, A., Thiry, M., and Wright, M., 1996, Evolution of landscapes in northern South Australia in relation to the distribution and formation of silcretes: Journal of the Geological Society, London, v. 153, p. 467–480

Stokes, W., 1968, Multiple parallel-truncation bedding planes—a feature of wind-deposited sandstone formations: Journal of Sedimentology Petrology, v. 38, no. 2, p. 510–515

Talbot, M.R., 1990, a Review of the palaeohydrological interpretation of carbon and oxygen isotopic ratios in primary lacustrine carbonates: Chemical Geology (Isotope Geoscience Section), v. 80, p. 261–279

Walker, T., 1979, Red color in dune sand, *in* Mckee E., *ed.*, A Study of Global Sand Seas: United States Government Printing Office, Washington D.C., p. 61–81

Yalin, M.S., 1964, Geometrical properties of sand waves: Journal of Hydraulic Division – Society of American Civil Engineers, v. 90, p. 105–119

APPENDIX A

BCC-2 Detrital Zircon Ages

							Isotope ratios							Apparent ages (Ma)							
	U	206Pb	U/Th	206Pb*	±	207Pb*	±	206Pb*	±	error	206Pb*	±	207Pb*	±	206Pb*	±	Best age	±	Conc
Sample	(ppm)	204Pb		207Pb*	(%)	235U*	(%)	238U	(%)	corr.	238U*	(Ma)	235U	(Ma)	207Pb*	(Ma)	(Ma)	(Ma)	(%)
1	372	5004	1.2	14.4475	3.0	0.3705	3.9	0.0388	2.4	0.63	245.5	5.9	320.0	10.7	905.2	62.6	245.5	5.9	NA
2	283	38176	1.4	19.1777	1.7	0.2823	3.1	0.0393	2.5	0.82	248.3	6.1	252.5	6.8	291.7	39.5	248.3	6.1	NA
3	363	6111	1.7	19.4997	3.7	0.2979	4.4	0.0421	2.2	0.51	266.0	5.8	264.8	10.2	253.6	86.1	266.0	5.8	NA
4	71	3735	0.8	20.1443	5.1	0.2937	5.9	0.0429	3.0	0.51	270.9	8.0	261.5	13.6	178.2	118.6	270.9	8.0	NA
5	424	8835	1.3	13.9639	1.3	0.4370	3.0	0.0443	2.7	0.91	279.2	7.4	368.1	9.2	975.0	25.5	279.2	7.4	NA
6	348	7863	3.0	19.3186	2.9	0.3303	4.0	0.0463	2.7	0.67	291.7	7.7	289.8	10.0	275.0	67.4	291.7	7.7	NA
7	1144	7704	2.0	14.8850	1.2	0.4479	2.6	0.0484	2.3	0.88	304.4	6.8	375.8	8.1	843.4	25.3	304.4	6.8	NA
8	530	5654	1.2	16.0545	1.6	0.4159	3.6	0.0484	3.2	0.89	304.8	9.5	353.1	10.6	684.0	33.9	304.8	9.5	NA
9	149	4347	1.6	16.7801	2.6	0.4014	3.6	0.0489	2.6	0.70	307.5	7.7	342.7	10.6	588.9	56.3	307.5	7.7	NA
10	382	14258	4.1	15.9590	1.4	0.4556	2.9	0.0527	2.5	0.87	331.3	8.1	381.2	9.2	696.8	30.1	331.3	8.1	NA
11	763	15626	11.3	16.7026	1.2	0.4479	3.2	0.0543	3.0	0.92	340.6	9.8	375.8	10.1	598.9	26.7	340.6	9.8	NA
12	753	6011	11.4	17.6434	1.2	0.4248	2.6	0.0544	2.3	0.88	341.2	7.5	359.5	7.8	479.0	26.5	341.2	7.5	NA
13	1023	7885	33.2	18.2938	1.3	0.4126	2.4	0.0547	2.1	0.85	343.6	6.9	350.7	7.2	398.5	28.3	343.6	6.9	NA
14	1385	5698	4.6	12.8178	1.7	0.5917	3.6	0.0550	3.2	0.88	345.2	10.8	471.9	13.7	1147.3	34.3	345.2	10.8	NA
15	113	5401	3.6	18.7196	2.2	0.4150	3.3	0.0563	2.4	0.74	353.4	8.4	352.5	9.8	346.7	50.2	353.4	8.4	NA
16	415	5564	1.6	17.9953	1.8	0.4478	3.5	0.0584	3.0	0.86	366.2	10.7	375.7	11.0	435.2	40.2	366.2	10.7	NA
17	358	8806	1.4	18.1038	1.9	0.4581	2.9	0.0601	2.2	0.76	376.5	8.0	382.9	9.2	421.8	42.1	376.5	8.0	NA
18	325	25957	1.6	17.6737	1.1	0.4752	2.7	0.0609	2.5	0.91	381.2	9.2	394.8	8.9	475.3	24.7	381.2	9.2	NA
19	183	5920	1.0	18.5547	1.8	0.4635	2.8	0.0624	2.1	0.76	390.1	8.1	386.7	9.0	366.6	40.8	390.1	8.1	NA
20	358	8937	73.5	18.3774	1.3	0.4719	2.4	0.0629	2.0	0.84	393.2	7.6	392.5	7.7	388.2	29.0	393.2	7.6	NA
21	235	6685	0.8	18.2944	2.9	0.4792	4.0	0.0636	2.7	0.68	397.3	10.4	397.5	13.0	398.4	64.7	397.3	10.4	NA
22	412	9391	1.4	16.8689	2.0	0.5208	3.2	0.0637	2.5	0.78	398.2	9.6	425.7	11.0	577.4	43.2	398.2	9.6	NA
23	714	17139	1.1	17.8789	1.4	0.4960	2.8	0.0643	2.4	0.87	401.8	9.5	409.0	9.4	449.6	30.4	401.8	9.5	89.4
24	153	6065	3.0	17.9255	2.9	0.4973	3.5	0.0647	2.1	0.58	403.9	8.1	409.9	11.9	443.9	63.7	403.9	8.1	91.0
25	791	31592	1.7	18.1007	1.1	0.4997	2.4	0.0656	2.2	0.90	409.6	8.6	411.5	8.1	422.2	23.5	409.6	8.6	97.0
26	375	6162	17.9	18.4479	3.4	0.4919	4.1	0.0658	2.2	0.54	410.9	8.7	406.2	13.6	379.6	76.8	410.9	8.7	108.2
27	290	7049	1.3	18.0162	1.5	0.5037	3.1	0.0658	2.7	0.88	410.9	10.8	414.2	10.4	432.6	32.4	410.9	10.8	95.0
28	234	6099	0.5	18.0214	2.1	0.5064	2.6	0.0662	1.6	0.59	413.1	6.2	416.0	9.0	432.0	47.4	413.1	6.2	95.6
29	238	12296	2.4	18.0628	1.6	0.5057	3.0	0.0662	2.6	0.85	413.5	10.3	415.5	10.4	426.9	35.6	413.5	10.3	96.9
30	107	3952	0.9	17.8835	1.6	0.5149	2.8	0.0668	2.3	0.82	416.8	9.4	421.8	9.8	449.1	35.9	416.8	9.4	92.8
31	388	10388	2.0	17.4927	2.0	0.5266	3.0	0.0668	2.3	0.75	416.9	9.1	429.6	10.6	497.9	44.2	416.9	9.1	83.7
32	94	5652	3.1	18.2249	2.6	0.5060	3.5	0.0669	2.4	0.67	417.3	9.6	415.7	12.0	406.9	58.2	417.3	9.6	102.6

33	578	15034	2.8	17.8287	1.2	0.5173	2.8	0.0669	2.5	0.90	417.4	10.0	423.3	9.6	455.9	27.3	417.4	10.0	91.6
34	475	40537	8.5	17.8172	1.1	0.5182	2.7	0.0670	2.4	0.90	417.8	9.8	423.9	9.3	457.4	25.4	417.8	9.8	91.4
35	369	23036	1.9	17.3458	1.0	0.5362	2.4	0.0675	2.1	0.90	420.8	8.7	435.9	8.4	516.5	22.5	420.8	8.7	81.5
36	206	8736	2.5	17.9368	1.4	0.5254	2.7	0.0683	2.2	0.84	426.2	9.3	428.7	9.3	442.5	31.8	426.2	9.3	96.3
37	371	9599	2.5	17.8488	1.5	0.5424	2.7	0.0702	2.3	0.83	437.4	9.6	440.0	9.7	453.4	33.5	437.4	9.6	96.5
38	268	7779	2.5	17.6687	1.5	0.5490	3.0	0.0704	2.5	0.86	438.3	10.8	444.4	10.6	475.9	33.0	438.3	10.8	92.1
39	237	32266	1.0	17.6330	1.4	0.5626	2.8	0.0719	2.5	0.87	447.9	10.6	453.2	10.4	480.3	31.5	447.9	10.6	93.2
40	140	6757	0.9	17.7677	1.7	0.5607	3.2	0.0723	2.7	0.84	449.8	11.8	452.0	11.7	463.5	38.5	449.8	11.8	97.0
41	362	17843	1.4	17.7335	1.5	0.5668	2.5	0.0729	2.0	0.80	453.6	8.8	456.0	9.1	467.8	32.8	453.6	8.8	97.0
42	110	5138	2.2	17.2399	4.2	0.6165	4.8	0.0771	2.4	0.49	478.7	10.9	487.7	18.5	530.0	91.3	478.7	10.9	90.3
43	177	47356	1.6	17.4943	1.6	0.6184	3.1	0.0785	2.6	0.85	486.9	12.3	488.8	11.9	497.8	35.1	486.9	12.3	97.8
44	623	10075	1.5	16.7496	1.0	0.6459	2.7	0.0785	2.5	0.93	487.0	11.9	506.0	10.8	592.8	21.1	487.0	11.9	82.1
45	190	6699	72.4	17.1494	1.7	0.6410	2.6	0.0797	2.0	0.75	494.5	9.4	503.0	10.4	541.5	37.7	494.5	9.4	91.3
46	658	42762	6.8	17.3165	1.2	0.6608	2.7	0.0830	2.4	0.89	514.0	11.8	515.1	10.8	520.2	26.6	514.0	11.8	98.8
47	77	5985	0.8	17.4530	2.1	0.6612	3.4	0.0837	2.7	0.80	518.1	13.6	515.3	13.8	503.0	45.2	518.1	13.6	103.0
48	293	11394	40.3	17.1469	1.4	0.6763	2.9	0.0841	2.5	0.86	520.6	12.4	524.5	11.7	541.8	31.5	520.6	12.4	96.1
49	334	8489	2.1	16.7287	1.2	0.6972	2.4	0.0846	2.1	0.86	523.5	10.3	537.1	10.0	595.5	26.7	523.5	10.3	87.9
50	70	5850	0.7	16.6978	1.8	0.7169	3.1	0.0868	2.6	0.82	536.7	13.3	548.8	13.4	599.5	39.0	536.7	13.3	89.5
51	228	15672	2.1	16.7811	1.6	0.7237	2.9	0.0881	2.4	0.82	544.2	12.3	552.8	12.3	588.7	35.7	544.2	12.3	92.4
52	297	21168	1.0	17.1113	1.2	0.7150	2.4	0.0887	2.0	0.85	548.1	10.7	547.7	10.1	546.3	27.2	548.1	10.7	100.3
53	77	5716	2.1	16.9525	1.9	0.7305	3.0	0.0898	2.3	0.76	554.5	12.0	556.9	12.8	566.7	42.2	554.5	12.0	97.8
54	106	8982	2.9	17.0832	2.0	0.7337	3.1	0.0909	2.4	0.76	560.9	12.8	558.7	13.5	549.9	44.7	560.9	12.8	102.0
55	152	6626	2.2	17.1223	2.2	0.7462	3.5	0.0927	2.7	0.78	571.3	14.9	566.0	15.1	544.9	47.1	571.3	14.9	104.8
56	193	10519	2.1	16.8954	1.6	0.7614	2.8	0.0933	2.3	0.82	575.0	12.7	574.8	12.4	574.0	35.6	575.0	12.7	100.2
57	254	8788	2.3	16.4228	2.1	0.7839	3.2	0.0934	2.4	0.76	575.4	13.3	587.7	14.2	635.4	44.5	575.4	13.3	90.6
58	64	6161	0.8	16.8536	2.2	0.7661	3.2	0.0936	2.4	0.73	577.1	13.0	577.5	14.3	579.4	48.2	577.1	13.0	99.6
59	83	6319	2.3	16.8230	1.7	0.7762	2.8	0.0947	2.2	0.78	583.3	12.2	583.3	12.4	583.3	37.6	583.3	12.2	100.0
60	388	11449	2.5	16.6373	1.3	0.7864	2.8	0.0949	2.5	0.89	584.4	13.8	589.1	12.5	607.4	27.8	584.4	13.8	96.2
61	456	12728	2.5	16.6327	1.5	0.7913	2.7	0.0955	2.3	0.84	587.7	12.9	591.9	12.2	608.0	31.5	587.7	12.9	96.7
62	605	19854	7.4	16.5219	1.0	0.7997	2.6	0.0958	2.4	0.92	589.9	13.6	596.7	11.8	622.4	22.5	589.9	13.6	94.8
63	85	7265	0.7	15.8997	2.5	0.8401	3.3	0.0969	2.1	0.64	596.1	12.1	619.2	15.3	704.7	53.7	596.1	12.1	84.6
64	315	9322	1.1	16.4229	2.1	0.8174	3.1	0.0974	2.3	0.75	598.9	13.3	606.6	14.2	635.4	44.4	598.9	13.3	94.3
65	406	14091	2.7	16.5405	1.3	0.8172	2.5	0.0980	2.2	0.85	602.9	12.4	606.5	11.6	620.0	28.9	602.9	12.4	97.2
66	133	7695	1.2	15.9970	1.4	0.8456	2.9	0.0981	2.6	0.88	603.3	14.7	622.2	13.5	691.7	29.5	603.3	14.7	87.2
67	130	5594	0.9	16.4636	3.0	0.8227	3.8	0.0982	2.3	0.62	604.1	13.3	609.6	17.2	630.1	63.7	604.1	13.3	95.9
68	62	6290	3.7	17.0548	2.8	0.7946	3.7	0.0983	2.3	0.64	604.4	13.5	593.8	16.5	553.5	61.9	604.4	13.5	109.2
69	474	610188	1.7	16.3480	1.1	0.8311	2.4	0.0985	2.1	0.90	605.8	12.4	614.2	11.0	645.2	22.7	605.8	12.4	93.9
70	178	5607	1.8	16.5702	1.4	0.8237	2.7	0.0990	2.3	0.86	608.5	13.6	610.1	12.6	616.1	30.6	608.5	13.6	98.8

71	161	7264	1.2	16.8392	1.7	0.8121	2.6	0.0992	2.1	0.78	609.6	12.0	603.6	12.1	581.3	36.1	609.6	12.0	104.9
72	362	20122	2.4	16.2621	1.3	0.8413	3.3	0.0992	3.0	0.91	609.9	17.7	619.8	15.4	656.5	28.9	609.9	17.7	92.9
73	100	6988	1.2	16.6087	1.9	0.8310	3.0	0.1001	2.3	0.76	615.0	13.4	614.1	13.8	611.1	41.9	615.0	13.4	100.6
74	656	24639	5.6	16.2848	1.0	0.8606	3.0	0.1016	2.9	0.95	624.1	17.1	630.5	14.2	653.5	20.5	624.1	17.1	95.5
75	238	5859	3.0	16.3686	1.7	0.8568	2.5	0.1017	1.8	0.71	624.5	10.5	628.4	11.6	642.5	37.2	624.5	10.5	97.2
76	76	6742	0.8	15.9262	2.5	0.8920	3.6	0.1030	2.5	0.72	632.2	15.3	647.5	17.0	701.1	52.8	632.2	15.3	90.2
77	72	8852	1.3	16.3234	2.4	0.8713	3.6	0.1032	2.7	0.75	632.9	16.2	636.3	16.9	648.5	50.7	632.9	16.2	97.6
78	332	8222	1.6	16.6356	1.2	0.8662	2.3	0.1045	2.0	0.85	640.8	12.0	633.5	10.9	607.6	26.1	640.8	12.0	105.5
79	325	6192	1.5	16.6893	1.2	0.8720	2.6	0.1055	2.4	0.89	646.8	14.5	636.6	12.5	600.6	26.0	646.8	14.5	107.7
80	138	7187	1.9	16.2635	1.4	0.9009	2.7	0.1063	2.4	0.87	651.0	14.7	652.2	13.2	656.3	29.3	651.0	14.7	99.2
81	314	6434	4.0	16.4079	1.3	0.8931	3.1	0.1063	2.8	0.90	651.1	17.4	648.0	14.9	637.4	28.9	651.1	17.4	102.2
82	331	39965	3.5	15.7031	1.2	0.9418	2.2	0.1073	1.8	0.84	656.8	11.3	673.8	10.6	731.1	24.8	656.8	11.3	89.8
83	288	170241	1.5	16.0544	1.1	0.9231	2.4	0.1075	2.2	0.89	658.1	13.6	664.0	11.9	684.0	23.7	658.1	13.6	96.2
84	162	5496	0.9	16.7082	2.0	0.8873	3.9	0.1075	3.3	0.86	658.3	20.9	644.9	18.5	598.2	43.2	658.3	20.9	110.1
85	203	9348	1.0	16.2905	1.5	0.9101	2.9	0.1075	2.5	0.85	658.4	15.4	657.1	13.9	652.8	32.3	658.4	15.4	100.9
86	467	8184	12.6	14.9639	1.0	1.0064	1.9	0.1092	1.6	0.84	668.2	10.2	707.0	9.8	832.4	21.9	668.2	10.2	80.3
87	506	12266	1.4	15.0000	1.2	1.0111	3.0	0.1100	2.8	0.91	672.8	17.6	709.4	15.4	827.4	25.6	672.8	17.6	81.3
88	316	9314	1.8	15.9936	1.2	0.9701	2.4	0.1125	2.1	0.86	687.4	13.7	688.5	12.2	692.1	26.6	687.4	13.7	99.3
89	183	14820	1.0	15.6825	1.3	0.9987	2.6	0.1136	2.3	0.87	693.6	15.1	703.2	13.4	733.9	27.8	693.6	15.1	94.5
90	115	48253	2.0	14.7703	1.6	1.1353	2.9	0.1216	2.3	0.82	739.9	16.4	770.3	15.4	859.5	33.7	739.9	16.4	86.1
91	232	17529	1.6	15.9389	1.4	1.0559	2.4	0.1221	1.9	0.81	742.4	13.6	731.8	12.4	699.4	29.4	742.4	13.6	106.1
92	140	7823	1.5	15.0697	1.4	1.1611	2.7	0.1269	2.3	0.85	770.2	16.5	782.5	14.6	817.7	29.6	770.2	16.5	94.2
93	615	159526	6.3	15.0905	0.8	1.1757	2.7	0.1287	2.6	0.95	780.3	18.9	789.3	14.8	814.8	17.4	780.3	18.9	95.8
94	369	25409	5.3	15.0742	1.1	1.2187	2.5	0.1332	2.2	0.89	806.3	16.9	809.2	13.9	817.1	23.4	806.3	16.9	98.7
95	102	17286	1.8	14.4044	1.2	1.3479	2.6	0.1408	2.3	0.89	849.3	18.1	866.6	14.9	911.3	23.9	849.3	18.1	93.2
96	626	71133	17.1	14.5500	1.1	1.3415	3.0	0.1416	2.8	0.93	853.5	22.2	863.9	17.4	890.6	22.6	853.5	22.2	95.8
97	62	5724	2.1	14.0925	2.5	1.5660	3.9	0.1601	3.0	0.77	957.1	27.0	956.8	24.4	956.2	51.1	956.2	51.1	100.1
98	704	21913	19.0	13.9389	1.2	1.4961	2.9	0.1512	2.7	0.91	908.0	22.5	928.8	17.8	978.6	24.9	978.6	24.9	92.8
99	1091	24153	3.9	13.9322	1.0	1.5553	2.6	0.1572	2.4	0.92	941.0	20.9	952.6	15.9	979.6	20.0	979.6	20.0	96.1
100	120	6230	1.4	13.9075	1.4	1.7092	3.0	0.1724	2.7	0.89	1025.4	25.5	1012.0	19.3	983.2	27.6	983.2	27.6	104.3
101	119	6262	3.2	13.8265	1.1	1.6909	2.5	0.1696	2.2	0.89	1009.7	20.8	1005.1	15.9	995.1	22.8	995.1	22.8	101.5
102	157	8886	3.8	13.8139	1.9	1.7117	3.2	0.1715	2.6	0.81	1020.3	24.1	1012.9	20.3	997.0	38.1	997.0	38.1	102.3
103	597	26685	4.4	13.8046	1.0	1.6017	2.4	0.1604	2.2	0.91	958.8	19.9	970.9	15.3	998.3	20.3	998.3	20.3	96.0
104	81	8422	0.5	13.7833	1.4	1.6684	2.5	0.1668	2.1	0.84	994.4	19.4	996.6	15.9	1001.4	27.4	1001.4	27.4	99.3
105	171	7726	1.7	13.7056	1.6	1.5294	4.4	0.1520	4.2	0.94	912.3	35.4	942.2	27.3	1012.9	31.5	1012.9	31.5	90.1
106	55	5421	2.2	13.6993	2.1	1.7225	3.1	0.1711	2.2	0.71	1018.4	20.5	1017.0	19.6	1013.8	43.4	1013.8	43.4	100.5
107	477	36848	4.8	13.6953	1.1	1.7897	3.0	0.1778	2.8	0.93	1054.8	27.0	1041.7	19.4	1014.4	21.9	1014.4	21.9	104.0
108	206	18078	1.5	13.6528	1.1	1.6040	2.6	0.1588	2.3	0.91	950.3	20.7	971.8	16.1	1020.7	21.4	1020.7	21.4	93.1

109	149	6145	2.4	13.6214	1.1	1.7768	3.1	0.1755	2.9	0.93	1042.5	28.3	1037.0	20.5	1025.4	22.9	1025.4	22.9	101.7
110	279	8910	1.3	13.5881	1.0	1.7295	3.1	0.1704	2.9	0.94	1014.6	27.3	1019.6	19.8	1030.3	20.9	1030.3	20.9	98.5
111	126	12176	2.9	13.5858	1.6	1.7891	2.7	0.1763	2.2	0.82	1046.7	21.5	1041.5	17.7	1030.7	31.6	1030.7	31.6	101.6
112	690	27295	143.7	13.5585	0.9	1.6527	2.5	0.1625	2.3	0.93	970.7	20.6	990.6	15.5	1034.7	18.0	1034.7	18.0	93.8
113	141	7184	3.0	13.5518	1.1	1.6017	2.3	0.1574	2.1	0.89	942.5	18.3	970.9	14.6	1035.7	21.5	1035.7	21.5	91.0
114	107	7493	1.7	13.5226	1.2	1.8553	2.9	0.1820	2.7	0.91	1077.7	26.4	1065.3	19.3	1040.1	24.8	1040.1	24.8	103.6
115	148	36188	1.8	13.5199	1.2	1.6876	2.4	0.1655	2.0	0.85	987.2	18.6	1003.9	15.2	1040.5	25.1	1040.5	25.1	94.9
116	220	11746	3.1	13.5193	1.1	1.7951	2.7	0.1760	2.5	0.92	1045.2	24.3	1043.7	17.9	1040.6	22.0	1040.6	22.0	100.4
117	473	23031	4.1	13.5070	1.0	1.7682	2.3	0.1732	2.1	0.90	1029.8	19.9	1033.9	15.1	1042.4	20.4	1042.4	20.4	98.8
118	725	30716	8.4	13.4755	1.0	1.7883	2.3	0.1748	2.0	0.90	1038.4	19.5	1041.2	14.7	1047.2	19.5	1047.2	19.5	99.2
119	664	40228	18.6	13.4130	0.9	1.8702	2.8	0.1819	2.7	0.95	1077.5	26.6	1070.6	18.6	1056.5	17.6	1056.5	17.6	102.0
120	254	89954	5.4	13.3971	0.9	1.8003	2.4	0.1749	2.2	0.92	1039.2	21.5	1045.6	15.8	1058.9	18.6	1058.9	18.6	98.1
121	168	5769	2.6	13.3953	1.4	1.7746	2.3	0.1724	1.9	0.81	1025.4	17.6	1036.2	14.9	1059.2	27.3	1059.2	27.3	96.8
122	221	19045	1.4	13.3658	1.3	1.6765	2.1	0.1625	1.7	0.79	970.8	15.2	999.7	13.6	1063.6	26.4	1063.6	26.4	91.3
123	134	8092	1.5	13.3548	1.3	1.8262	2.7	0.1769	2.4	0.88	1049.9	23.3	1054.9	17.9	1065.3	26.2	1065.3	26.2	98.6
124	217	12773	1.3	13.3245	1.1	1.8821	2.4	0.1819	2.1	0.90	1077.3	21.3	1074.8	15.9	1069.9	21.1	1069.9	21.1	100.7
125	305	33363	45.0	13.2872	1.0	1.9219	2.2	0.1852	2.0	0.89	1095.4	19.7	1088.7	14.6	1075.5	19.8	1075.5	19.8	101.9
126	134	15464	2.0	13.2398	1.2	1.8916	2.5	0.1816	2.3	0.89	1075.9	22.4	1078.1	16.9	1082.6	23.5	1082.6	23.5	99.4
127	126	6372	2.6	13.2395	1.4	1.9227	2.5	0.1846	2.1	0.83	1092.2	20.7	1089.0	16.6	1082.7	27.8	1082.7	27.8	100.9
128	36	4375	1.5	13.2154	1.9	1.8047	2.9	0.1730	2.3	0.77	1028.5	21.6	1047.1	19.1	1086.4	37.2	1086.4	37.2	94.7
129	109	25972	3.6	13.2033	1.3	1.8407	2.9	0.1763	2.6	0.90	1046.5	25.4	1060.1	19.2	1088.2	25.2	1088.2	25.2	96.2
130	661	18955	4.1	13.1581	0.9	1.6305	2.5	0.1556	2.3	0.93	932.3	19.9	982.0	15.5	1095.1	17.6	1095.1	17.6	85.1
131	49	6063	4.0	13.1492	1.8	1.8671	2.9	0.1781	2.3	0.80	1056.3	22.7	1069.5	19.3	1096.4	35.1	1096.4	35.1	96.3
132	388	13733	3.1	13.0886	1.0	1.9483	2.6	0.1849	2.4	0.92	1094.0	24.1	1097.9	17.5	1105.7	20.9	1105.7	20.9	98.9
133	83	7833	1.3	13.0861	1.2	1.9821	2.6	0.1881	2.3	0.88	1111.2	23.1	1109.4	17.3	1106.0	24.2	1106.0	24.2	100.5
134	214	47319	3.2	13.0815	1.1	2.0239	2.4	0.1920	2.1	0.89	1132.3	22.3	1123.6	16.4	1106.7	22.3	1106.7	22.3	102.3
135	311	22281	1.5	13.0550	1.0	1.7783	2.4	0.1684	2.1	0.91	1003.2	19.9	1037.6	15.4	1110.8	20.0	1110.8	20.0	90.3
136	265	12994	5.2	12.9964	1.3	1.9045	2.5	0.1795	2.2	0.86	1064.4	21.2	1082.7	16.7	1119.8	25.3	1119.8	25.3	95.1
137	157	8713	2.5	12.9866	1.2	1.9838	2.9	0.1868	2.7	0.91	1104.3	27.1	1110.0	19.9	1121.3	24.8	1121.3	24.8	98.5
138	64	16600	0.8	12.9697	1.4	1.9726	2.7	0.1856	2.4	0.86	1097.2	23.8	1106.2	18.5	1123.8	28.1	1123.8	28.1	97.6
139	217	17010	1.6	12.9259	1.1	1.9557	2.0	0.1833	1.6	0.84	1085.2	16.4	1100.4	13.2	1130.6	21.5	1130.6	21.5	96.0
140	816	38326	4.3	12.8892	1.0	1.7939	2.8	0.1677	2.6	0.94	999.4	24.3	1043.2	18.2	1136.3	19.3	1136.3	19.3	88.0
141	181	7796	2.1	12.8552	2.1	2.0783	3.2	0.1938	2.4	0.76	1141.7	25.3	1141.7	21.9	1141.5	41.7	1141.5	41.7	100.0
142	641	22337	5.0	12.8483	0.8	2.0087	2.5	0.1872	2.4	0.95	1106.1	23.9	1118.5	16.8	1142.6	15.8	1142.6	15.8	96.8
143	210	8797	4.1	12.7935	1.0	2.0465	2.6	0.1899	2.4	0.92	1120.8	24.3	1131.1	17.6	1151.1	20.5	1151.1	20.5	97.4
144	64	5249	2.7	12.7825	1.4	1.9410	3.2	0.1799	2.9	0.90	1066.7	28.5	1095.3	21.6	1152.7	27.7	1152.7	27.7	92.5
145	206	6974	4.1	12.7621	1.6	2.1384	2.9	0.1979	2.3	0.82	1164.2	25.0	1161.3	19.7	1155.9	32.2	1155.9	32.2	100.7
146	98	40993	2.0	12.7406	1.6	1.8078	3.0	0.1670	2.6	0.86	995.8	24.2	1048.3	19.9	1159.3	31.0	1159.3	31.0	85.9

147	33	23413	0.7	12.6737	1.9	1.9071	3.2	0.1753	2.5	0.79	1041.2	23.9	1083.6	21.0	1169.7	38.5	1169.7	38.5	89.0
148	130	9767	2.5	12.5434	1.2	2.1821	2.3	0.1985	2.0	0.86	1167.3	21.5	1175.3	16.2	1190.1	23.2	1190.1	23.2	98.1
149	110	76859	1.3	12.4681	1.2	2.1138	3.1	0.1911	2.8	0.92	1127.6	29.4	1153.3	21.2	1202.0	23.3	1202.0	23.3	93.8
150	454	14892	2.8	12.4062	1.2	2.1426	2.6	0.1928	2.4	0.90	1136.4	24.7	1162.7	18.3	1211.9	22.8	1211.9	22.8	93.8
151	649	23512	1.9	12.3719	1.1	2.2483	2.8	0.2017	2.6	0.92	1184.6	27.9	1196.3	19.8	1217.3	22.1	1217.3	22.1	97.3
152	270	19140	2.9	12.3597	1.0	2.1253	2.4	0.1905	2.1	0.90	1124.1	22.1	1157.0	16.4	1219.2	19.9	1219.2	19.9	92.2
153	179	10822	3.8	12.3036	1.5	2.3797	3.1	0.2124	2.7	0.88	1241.3	30.4	1236.5	22.0	1228.1	28.9	1228.1	28.9	101.1
154	114	14262	2.3	12.2699	1.3	2.2543	3.2	0.2006	2.9	0.91	1178.6	31.0	1198.1	22.3	1233.5	26.0	1233.5	26.0	95.5
155	437	38445	3.2	12.2251	0.9	2.2423	2.2	0.1988	2.0	0.91	1168.9	21.8	1194.4	15.7	1240.7	18.3	1240.7	18.3	94.2
156	56	7229	1.7	12.1384	1.4	2.4134	2.5	0.2125	2.2	0.84	1242.0	24.3	1246.6	18.3	1254.6	26.6	1254.6	26.6	99.0
157	308	8355	5.7	12.1114	1.1	2.5011	3.2	0.2197	3.1	0.94	1280.3	35.4	1272.4	23.5	1259.0	21.2	1259.0	21.2	101.7
158	175	5640	0.6	11.8930	1.2	2.5932	2.9	0.2237	2.7	0.92	1301.3	31.9	1298.7	21.6	1294.5	22.6	1294.5	22.6	100.5
159	162	7292	1.8	11.8772	1.2	2.6041	3.1	0.2243	2.9	0.93	1304.7	34.0	1301.8	22.8	1297.0	22.6	1297.0	22.6	100.6
160	242	49082	3.9	11.7937	1.2	2.5741	2.5	0.2202	2.2	0.88	1282.8	26.0	1293.3	18.5	1310.8	22.8	1310.8	22.8	97.9
161	629	48104	0.8	11.6484	0.8	2.6372	2.7	0.2228	2.5	0.95	1296.6	29.7	1311.1	19.6	1334.8	15.7	1334.8	15.7	97.1
162	289	19647	3.4	11.5197	0.9	2.9449	2.1	0.2460	1.9	0.91	1418.0	24.5	1393.5	16.1	1356.2	17.2	1356.2	17.2	104.6
163	194	27450	3.0	11.3196	1.0	2.8887	2.7	0.2372	2.5	0.93	1371.9	31.2	1379.0	20.4	1389.9	18.5	1389.9	18.5	98.7
164	95	19027	1.4	11.2415	1.1	2.5981	2.3	0.2118	2.0	0.88	1238.6	22.2	1300.1	16.5	1403.2	20.8	1403.2	20.8	88.3
165	328	16329	1.9	11.1319	1.0	3.1058	2.5	0.2508	2.3	0.92	1442.4	30.1	1434.1	19.5	1421.9	19.4	1421.9	19.4	101.4
166	170	8516	1.1	11.0907	1.1	2.5540	2.7	0.2054	2.5	0.91	1204.5	27.4	1287.6	20.0	1429.0	21.6	1429.0	21.6	84.3
167	106	6282	3.2	11.0896	1.3	3.0041	2.5	0.2416	2.2	0.87	1395.1	27.6	1408.7	19.4	1429.2	24.3	1429.2	24.3	97.6
168	129	8385	1.4	11.0817	1.0	2.5404	1.7	0.2042	1.4	0.81	1197.7	15.4	1283.7	12.6	1430.6	19.1	1430.6	19.1	83.7
169	324	15829	2.3	11.0175	1.0	3.3034	2.9	0.2640	2.7	0.94	1510.1	36.8	1481.9	22.6	1441.7	18.6	1441.7	18.6	104.7
170	210	15734	0.9	11.0048	1.2	3.2037	2.3	0.2557	2.0	0.87	1467.8	26.9	1458.0	18.2	1443.9	21.9	1443.9	21.9	101.7
171	369	18085	1.1	10.9984	1.0	3.0418	2.3	0.2426	2.1	0.90	1400.4	26.2	1418.2	17.6	1444.9	18.8	1444.9	18.8	96.9
172	136	8530	1.4	10.9793	0.9	3.0212	3.3	0.2406	3.1	0.96	1389.7	39.0	1413.0	24.9	1448.3	17.9	1448.3	17.9	96.0
173	187	46409	1.6	10.9497	1.0	3.1395	2.2	0.2493	2.0	0.90	1435.0	25.5	1442.4	17.0	1453.4	18.2	1453.4	18.2	98.7
174	257	7914	2.5	10.9428	1.1	2.9936	2.7	0.2376	2.5	0.92	1374.1	30.8	1406.0	20.6	1454.6	20.3	1454.6	20.3	94.5
175	379	22735	1.6	10.9394	1.1	3.0031	2.5	0.2383	2.2	0.90	1377.7	27.9	1408.4	19.1	1455.2	21.2	1455.2	21.2	94.7
176	78	5411	1.8	10.9198	2.1	2.9963	2.9	0.2373	2.0	0.70	1372.6	24.9	1406.7	22.0	1458.6	39.4	1458.6	39.4	94.1
177	265	45169	2.5	10.8054	0.9	3.1950	1.9	0.2504	1.7	0.87	1440.5	21.8	1456.0	15.0	1478.6	17.9	1478.6	17.9	97.4
178	253	8738	3.6	10.7591	1.0	3.3143	2.6	0.2586	2.4	0.92	1482.8	31.5	1484.4	20.2	1486.7	19.3	1486.7	19.3	99.7
179	170	18178	0.8	10.7142	1.0	3.4738	2.9	0.2699	2.7	0.93	1540.5	37.2	1521.3	22.9	1494.7	19.6	1494.7	19.6	103.1
180	123	9385	3.1	10.6590	1.2	3.2941	2.7	0.2547	2.5	0.90	1462.4	32.1	1479.7	21.1	1504.4	21.8	1504.4	21.8	97.2
181	73	6711	1.2	10.6262	1.4	3.2423	2.7	0.2499	2.3	0.85	1437.9	29.2	1467.3	20.7	1510.2	26.7	1510.2	26.7	95.2
182	173	44198	2.3	10.5430	1.1	3.4494	2.5	0.2638	2.3	0.91	1509.1	30.5	1515.7	19.7	1525.1	19.9	1525.1	19.9	99.0
183	521	37963	2.7	10.4688	0.9	3.3917	2.1	0.2575	1.9	0.90	1477.1	25.1	1502.5	16.5	1538.4	16.9	1538.4	16.9	96.0
184	141	12654	1.4	10.4082	1.0	3.0740	2.4	0.2320	2.2	0.90	1345.2	26.4	1426.2	18.5	1549.3	19.4	1549.3	19.4	86.8

185	115	6147	1.3	10.3210	1.5	3.4561	2.5	0.2587	2.0	0.79	1483.2	26.0	1517.3	19.7	1565.1	29.0	1565.1	29.0	94.8
186	212	20565	0.9	10.2639	1.0	3.6711	2.1	0.2733	1.9	0.89	1557.4	26.0	1565.1	16.9	1575.5	18.1	1575.5	18.1	98.9
187	287	11314	1.4	10.1522	1.0	3.3353	2.3	0.2456	2.1	0.91	1415.6	26.4	1489.4	17.9	1595.9	18.0	1595.9	18.0	88.7
188	123	13924	1.2	10.1086	1.0	3.5905	2.5	0.2632	2.3	0.91	1506.4	30.7	1547.4	19.9	1604.0	18.9	1604.0	18.9	93.9
189	521	24283	9.1	10.1055	0.8	3.0979	2.7	0.2270	2.6	0.95	1319.0	30.7	1432.2	20.8	1604.5	15.8	1604.5	15.8	82.2
190	294	26117	2.3	10.0996	0.9	3.8630	2.2	0.2830	2.0	0.92	1606.2	28.7	1606.0	17.7	1605.6	16.1	1605.6	16.1	100.0
191	147	9106	1.6	10.0212	1.0	3.8399	2.3	0.2791	2.0	0.89	1586.8	28.2	1601.2	18.2	1620.1	19.4	1620.1	19.4	97.9
192	74	10801	0.9	9.9250	1.5	3.9521	3.0	0.2845	2.6	0.87	1613.9	36.7	1624.4	24.0	1638.1	27.5	1638.1	27.5	98.5
193	249	15656	2.0	9.9177	1.2	3.9201	3.0	0.2820	2.8	0.91	1601.3	39.1	1617.8	24.4	1639.4	22.7	1639.4	22.7	97.7
194	262	20341	3.9	9.9086	1.0	4.2556	2.2	0.3058	2.0	0.89	1720.1	29.5	1684.8	18.2	1641.1	19.0	1641.1	19.0	104.8
195	113	9475	0.9	9.8763	1.1	3.9058	3.0	0.2798	2.7	0.92	1590.2	38.5	1614.9	24.0	1647.2	21.3	1647.2	21.3	96.5
196	135	45856	1.0	9.8340	0.9	3.9211	2.0	0.2797	1.8	0.89	1589.7	25.7	1618.0	16.5	1655.1	17.2	1655.1	17.2	96.0
197	210	33432	1.0	9.7577	0.9	3.8546	2.4	0.2728	2.2	0.93	1554.9	30.6	1604.2	19.3	1669.6	16.8	1669.6	16.8	93.1
198	564	33723	5.3	9.6799	0.9	4.3264	2.4	0.3037	2.2	0.92	1709.8	33.4	1698.4	19.9	1684.3	17.5	1684.3	17.5	101.5
199	102	11598	1.0	9.5490	1.1	4.3949	2.7	0.3044	2.4	0.91	1713.0	36.3	1711.4	22.0	1709.4	20.4	1709.4	20.4	100.2
200	251	17463	3.2	9.5184	1.1	4.3159	2.8	0.2979	2.5	0.92	1681.1	37.4	1696.4	22.7	1715.3	20.1	1715.3	20.1	98.0
201	808	33534	2.1	9.4932	0.9	4.2150	2.4	0.2902	2.2	0.92	1642.6	31.7	1677.0	19.6	1720.2	17.3	1720.2	17.3	95.5
202	631	38016	2.8	9.4718	0.8	3.9941	2.7	0.2744	2.6	0.96	1563.0	36.5	1633.0	22.3	1724.4	14.7	1724.4	14.7	90.6
203	265	19349	3.1	9.4503	1.0	4.4435	2.6	0.3046	2.4	0.93	1713.9	35.6	1720.5	21.1	1728.5	17.5	1728.5	17.5	99.2
204	581	30390	2.4	9.4156	1.1	4.4408	2.6	0.3033	2.3	0.90	1707.4	35.2	1720.0	21.6	1735.3	20.5	1735.3	20.5	98.4
205	613	30075	2.6	9.4061	1.0	4.5256	2.8	0.3087	2.6	0.93	1734.5	39.5	1735.7	23.1	1737.1	18.1	1737.1	18.1	99.8
206	483	41090	2.0	9.3911	0.8	4.0637	2.3	0.2768	2.1	0.93	1575.1	29.3	1647.0	18.4	1740.1	15.2	1740.1	15.2	90.5
207	124	7850	1.6	9.2236	1.0	4.7599	2.3	0.3184	2.0	0.89	1782.0	31.8	1777.9	19.2	1773.0	19.0	1773.0	19.0	100.5
208	237	13826	2.1	9.1528	1.5	4.5844	3.1	0.3043	2.7	0.87	1712.7	40.0	1746.4	25.6	1787.0	27.9	1787.0	27.9	95.8
209	133	20797	3.3	9.1187	1.1	4.9149	2.4	0.3250	2.2	0.90	1814.3	34.6	1804.8	20.6	1793.8	19.6	1793.8	19.6	101.1
210	228	15674	2.3	9.1095	1.1	4.8995	2.6	0.3237	2.4	0.91	1807.8	37.9	1802.2	22.3	1795.7	20.0	1795.7	20.0	100.7
211	253	23097	1.8	9.1073	1.0	4.8429	2.5	0.3199	2.3	0.91	1789.2	35.8	1792.4	21.2	1796.1	18.9	1796.1	18.9	99.6
212	330	44847	2.6	9.0780	1.0	5.0183	2.6	0.3304	2.3	0.92	1840.4	37.5	1822.4	21.6	1802.0	18.4	1802.0	18.4	102.1
213	126	22772	1.4	9.0623	1.2	4.6503	2.4	0.3056	2.2	0.88	1719.3	32.5	1758.4	20.4	1805.1	20.9	1805.1	20.9	95.2
214	235	26646	1.3	9.0326	0.8	4.8571	2.1	0.3182	1.9	0.92	1780.9	29.7	1794.9	17.5	1811.1	15.1	1811.1	15.1	98.3
215	290	22584	1.9	9.0267	0.8	4.8790	2.9	0.3194	2.8	0.96	1786.9	43.5	1798.6	24.5	1812.3	14.7	1812.3	14.7	98.6
216	316	25998	0.8	9.0197	0.9	4.7876	2.1	0.3132	2.0	0.92	1756.4	30.3	1782.7	18.0	1813.7	15.5	1813.7	15.5	96.8
217	351	36829	1.8	8.9138	0.8	5.0260	2.6	0.3249	2.5	0.95	1813.7	38.9	1823.7	22.0	1835.1	14.8	1835.1	14.8	98.8
218	278	22761	1.0	8.8403	0.9	5.1442	2.2	0.3298	2.1	0.92	1837.5	32.9	1843.4	19.0	1850.1	15.9	1850.1	15.9	99.3
219	309	27195	0.9	8.7442	0.9	5.2392	2.4	0.3323	2.2	0.93	1849.3	36.1	1859.0	20.7	1869.8	16.5	1869.8	16.5	98.9
220	314	46053	1.9	8.6810	0.9	5.5438	2.2	0.3490	2.0	0.91	1930.0	33.1	1907.4	18.7	1882.9	16.0	1882.9	16.0	102.5
221	269	25578	1.9	8.4021	1.1	5.5563	2.2	0.3386	1.9	0.87	1879.9	31.0	1909.4	18.8	1941.5	19.4	1941.5	19.4	96.8
222	328	31855	3.8	8.3945	0.9	4.7360	3.1	0.2883	3.0	0.96	1633.2	43.6	1773.6	26.4	1943.1	15.5	1943.1	15.5	84.1

223	387	40050	3.8	8.2927	1.0	5.7089	2.7	0.3434	2.5	0.93	1902.8	40.7	1932.7	23.0	1964.9	17.5	1964.9	17.5	96.8
224	79	32763	1.8	8.1680	1.3	5.5574	2.8	0.3292	2.5	0.89	1834.6	40.3	1909.5	24.4	1991.9	23.0	1991.9	23.0	92.1
225	56	19373	3.5	8.1614	1.2	6.1734	2.9	0.3654	2.6	0.91	2007.8	44.8	2000.7	25.1	1993.3	21.6	1993.3	21.6	100.7
226	183	47513	1.6	8.0895	1.1	5.4389	2.4	0.3191	2.1	0.89	1785.3	33.3	1891.0	20.5	2009.1	19.0	2009.1	19.0	88.9
227	98	27344	2.3	7.9750	1.2	5.9211	2.5	0.3425	2.2	0.88	1898.6	35.8	1964.3	21.5	2034.3	20.9	2034.3	20.9	93.3
228	293	24929	1.0	7.9619	0.9	6.1034	2.1	0.3524	1.9	0.90	1946.2	31.9	1990.7	18.4	2037.2	16.1	2037.2	16.1	95.5
229	246	43373	2.2	7.8887	1.1	6.2582	2.7	0.3581	2.5	0.91	1973.0	42.6	2012.6	24.1	2053.6	19.9	2053.6	19.9	96.1
230	273	24081	1.7	7.8510	0.8	6.6528	2.7	0.3788	2.5	0.95	2070.7	44.9	2066.4	23.5	2062.0	14.1	2062.0	14.1	100.4
231	142	12570	2.3	7.8127	1.0	6.5573	2.6	0.3716	2.4	0.92	2036.7	41.9	2053.6	23.0	2070.6	17.8	2070.6	17.8	98.4
232	230	29187	0.9	7.7923	0.8	6.6709	2.0	0.3770	1.8	0.91	2062.3	32.2	2068.8	17.7	2075.2	14.6	2075.2	14.6	99.4
233	128	51197	1.2	7.6793	1.0	6.6489	2.3	0.3703	2.1	0.90	2030.9	36.0	2065.9	20.3	2100.9	17.6	2100.9	17.6	96.7
234	198	31243	1.5	7.5602	0.8	6.8979	1.9	0.3782	1.8	0.91	2068.0	31.3	2098.4	17.2	2128.3	13.9	2128.3	13.9	97.2
235	266	37997	2.1	7.5542	1.0	6.9785	2.7	0.3823	2.5	0.92	2087.2	43.8	2108.7	23.6	2129.7	17.9	2129.7	17.9	98.0
236	360	23823	1.9	7.4673	0.9	6.7957	2.9	0.3680	2.7	0.95	2020.2	47.2	2085.2	25.5	2149.9	16.4	2149.9	16.4	94.0
237	49	12960	0.8	6.3500	1.0	9.9006	3.2	0.4560	3.0	0.94	2421.7	60.1	2425.6	29.1	2428.8	17.5	2428.8	17.5	99.7
238	154	17443	4.4	5.5369	0.9	12.0408	2.5	0.4835	2.3	0.93	2542.6	49.3	2607.6	23.7	2658.4	15.7	2658.4	15.7	95.6
239	71	609142	1.2	5.5074	0.7	12.9269	2.3	0.5163	2.2	0.95	2683.7	48.7	2674.3	22.0	2667.3	12.3	2667.3	12.3	100.6
240	244	21420	1.7	5.4668	0.8	11.8874	2.3	0.4713	2.1	0.93	2489.4	44.3	2595.6	21.6	2679.5	13.8	2679.5	13.8	92.9
241	435	37988	1.5	5.4233	0.9	12.5370	2.0	0.4931	1.8	0.88	2584.2	37.8	2645.5	18.9	2692.8	15.6	2692.8	15.6	96.0
242	152	66075	2.2	5.2932	1.1	13.8585	2.2	0.5320	1.9	0.88	2750.0	43.1	2740.1	20.8	2732.8	17.4	2732.8	17.4	100.6
243	505	41444	2.1	5.2545	0.9	12.8364	2.3	0.4892	2.1	0.92	2567.1	44.9	2667.7	21.8	2744.9	15.2	2744.9	15.2	93.5
244	203	19544	6.1	5.1022	1.1	12.7661	2.8	0.4724	2.6	0.92	2494.1	52.7	2662.5	26.0	2793.1	17.4	2793.1	17.4	89.3
245	154	15830	0.7	5.0249	0.8	15.1417	2.6	0.5518	2.4	0.95	2832.7	56.2	2824.2	24.4	2818.1	12.5	2818.1	12.5	100.5
246	433	64648	1.8	4.8625	0.9	15.6606	2.5	0.5523	2.4	0.94	2834.7	54.0	2856.3	23.9	2871.6	14.0	2871.6	14.0	98.7
247	373	55189	41.3	4.8491	0.7	15.0508	2.2	0.5293	2.1	0.94	2738.6	46.6	2818.5	21.1	2876.1	11.9	2876.1	11.9	95.2
248	50	20959	1.7	4.5551	1.0	17.9525	2.4	0.5931	2.2	0.91	3001.9	53.4	2987.2	23.4	2977.3	15.9	2977.3	15.9	100.8

APPENDIX B

Detrital Zircon $^{206}Pb/^{238}U$ data for
BCC Mudstone (20.35 m)

Age determined by $^{206}Pb/^{238}U$	± 2σ abs
566.7	3.6
420.21	0.37
324.98	0.26
318.9	1.5

APPENDIX C

Volcanic Ash $^{206}Pb/^{238}U$ data for the
Ralston Creek Formation (155.4 m)

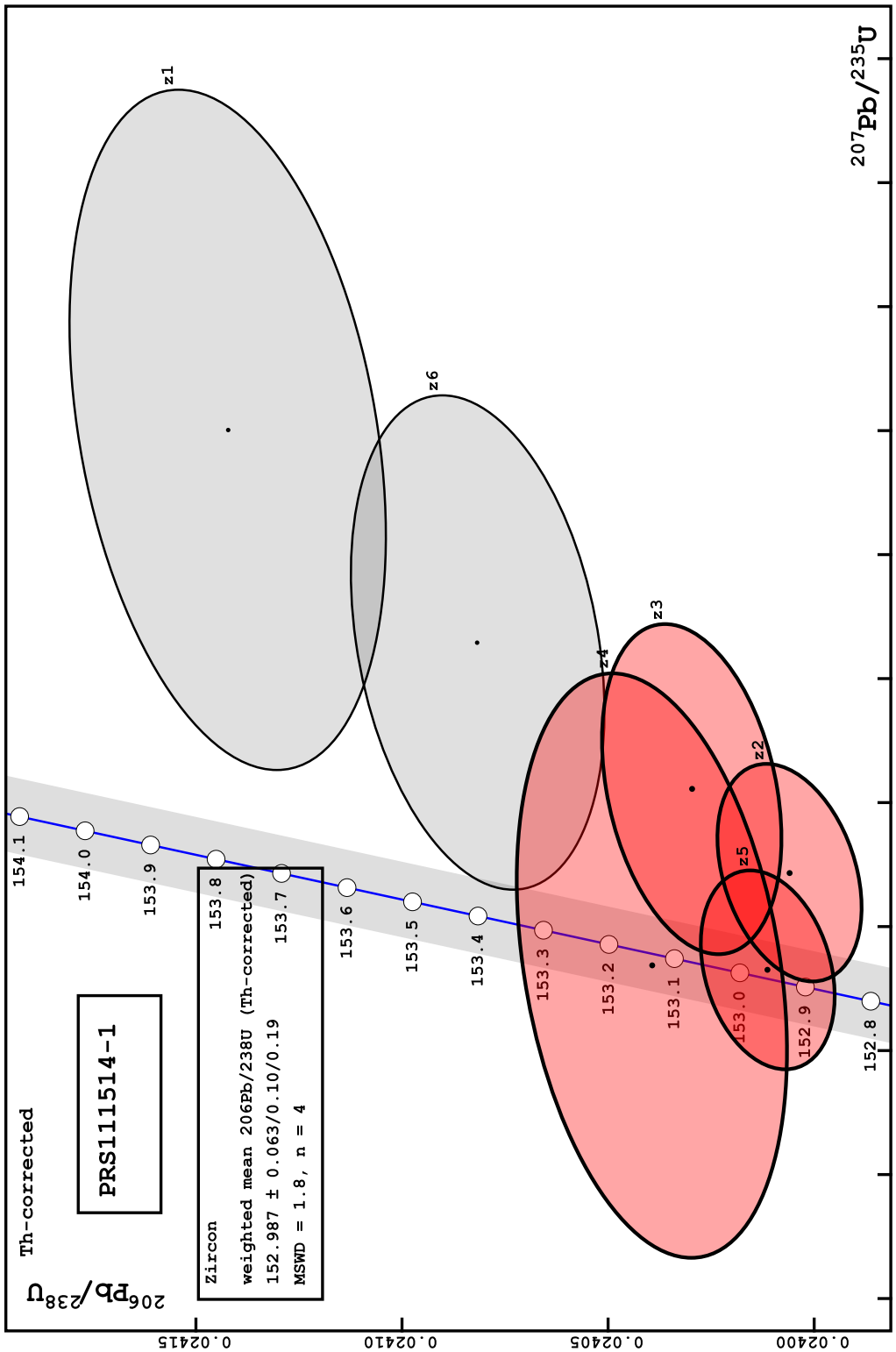

						Ratios						Ages (Ma)						
Sample Fractions (a)	Pb(c) (pg) (b)	Pb* / Pb(c)	Th / U	206 Pb / 204 Pb (c)	208 Pb / 206 Pb (d)	206 Pb / 238 U (e)	err (2s%)	207 Pb / 235 U (e)	err (2s%)	207 Pb / 206 Pb (e)	err (2s%)	206 Pb / 238 U	err (2s)	207 Pb / 235 U	err (2s)	207 Pb / 206 Pb	err (2s)	corr. coef.
PRC 155.4 m																		
Zircon 1	0.2	12.3	1.09	642.1	0.348	0.024142	(.16)	0.16701	(1.64)	0.05019	(1.60)	153.78	0.24	156.8	2.4	203	37	0.311
Zircon 2	0.2	37.6	1.03	1963.7	0.327	0.024006	(.07)	0.16343	(.54)	0.04940	(.52)	**152.92**	**0.11**	153.71	0.77	166	12	0.321
Zircon 3	0.2	24.5	1.05	1280.4	0.333	0.024030	(.09)	0.16411	(.81)	0.04955	(.79)	**153.07**	**0.14**	154.3	1.2	173	18	0.299
Zircon 4	0.3	13.7	1.03	727.3	0.329	0.024039	(.14)	0.16269	(1.45)	0.04910	(1.41)	**153.13**	**0.21**	153.1	2.1	152	33	0.293
Zircon 5	0.2	44.0	1.08	2268.7	0.342	0.024011	(.07)	0.16265	(.49)	0.04915	(.48)	**152.96**	**0.10**	153.02	0.70	154	11	0.263
Zircon 6	0.2	17.1	1.08	889.7	0.344	0.024082	(.13)	0.16529	(1.21)	0.04980	(1.18)	153.40	0.19	155.3	1.7	185	27	0.279

APPENDIX D

BCC Stromatolite and Lykins Formation

Stable Isotope Data

Section	$\delta^{13}C$	$\delta^{18}O$	Sample ID
BCC	-2.37	-2.08	5.66
BCC	6.19	4.35	5.86
BCC	6.03	4.24	6.02
BCC	6.13	2.73	6.21
BCC	5.57	2.72	6.40
BCC	5.61	3.03	6.57
BCC	5.18	2.57	6.72
BCC	5.50	3.52	6.85
BCC	3.92	2.44	7.02
BCC	4.76	3.13	7.18
BCC	2.13	3.09	9.70
BCC	1.55	2.91	9.84
BCC	2.68	1.76	9.94
BCC	2.60	2.36	10.09
BCC	3.85	2.46	10.26
BCC	3.61	2.66	10.47
BCC	3.74	2.34	10.51
BCC	5.15	2.74	10.64
BCC	5.33	1.97	10.83
BCC	4.56	2.39	10.96
BCC	3.63	2.16	11.06
BCC	2.80	1.35	11.25
BCC	2.55	0.72	11.59
BCC	2.90	-0.02	11.72
BCC	-6.92	-0.09	11.89
BCC	-7.16	0.77	12.06
BCC	-5.92	-3.97	12.18
BCC	-7.27	0.87	12.31
BCC	-6.75	0.02	12.45
BCC	-7.25	1.70	12.57
Lykins	1.05	3.62	18.81
Lykins	0.17	-0.36	19.07
Lykins	1.77	0.19	19.45
Lykins	1.60	0.34	19.53
Lykins	1.15	0.52	19.68
Lykins	0.98	-1.89	19.85
Lykins	0.92	-2.05	19.94
Lykins	0.97	-2.04	20.11

APPENDIX E

Ralston Creek and Morrison
Strata Stable Isotope Data

Section	$\delta^{13}C$	$\delta^{18}O$	Sample ID
PFS	-7.03	-7.27	0.35
PFS	-3.84	-8.57	0.47
PFS	-2.57	-6.46	0.82
PFS	-1.42	-5.20	1.02
PFS	-2.24	-6.11	1.29
PFS	-3.90	-7.09	1.41
PFS	-4.05	-7.24	1.56
PFS	-3.39	-6.62	1.72
PFS	-3.15	-6.42	2.11
PFS	-3.59	-6.89	2.29
PFS	-2.65	-6.35	2.92
PFS	-4.88	-13.09	2.95
PFS	-4.45	-7.54	3.01
PFS	-3.72	-6.23	3.06
PFS	-3.11	-6.58	3.24
PFS	-3.19	-6.34	3.35
PRC	-5.39	-9.11	9.06
PRC	-5.53	-9.09	9.27
PRC	-6.68	-9.94	9.95
PRC	-4.12	-8.62	10.55
PRC	-4.63	-8.85	11.34
PRC	-2.56	-8.28	13.67
PRC	-3.22	-9.10	14.02
PRC	-1.41	-9.82	14.54
PRC	-2.95	-8.10	14.71
PRC	-1.98	-9.91	14.85
PRC	-4.45	-8.37	18.86
RROS	-3.43	-6.88	52.26
RROS	-2.86	-7.19	52.31
RROS	-4.67	-7.53	52.48
RROS	-2.96	-8.09	52.74
RROS	-2.53	-8.33	52.85
RROS	-2.01	-7.85	52.91
RROS	-1.63	-7.71	53.05
RROS	-1.35	-7.48	53.17
RROS	-1.35	-7.41	53.27
RROS	-1.60	-7.63	53.56
RROS	-1.87	-8.05	53.70

RROS	-1.62	-7.93	53.86
RROS	-1.63	-5.98	53.96
RROS	-2.09	-7.17	54.11
RROS	-1.27	-7.86	54.22
RROS	-1.92	-7.99	54.70
RROS	-1.98	-7.38	54.79
RROS	-1.66	-7.07	54.94
RROS	-1.47	-7.11	55.14